

Strongly Coupled Data Assimilation Experiments with Linearized Ocean–Atmosphere Balance Relationships[©]

ANDREA STORTO^a

Centro Euro-Mediterraneo sui Cambiamenti Climatici, Bologna, Italy

MATTHEW J. MARTIN

Met Office, Exeter, United Kingdom

BRUNO DEREMBLE

Laboratoire de Météorologie Dynamique, École Normale Supérieure, Paris, France

SIMONA MASINA

Centro Euro-Mediterraneo sui Cambiamenti Climatici, and Istituto Nazionale di Geofisica e Vulcanologia, Bologna, Italy

(Manuscript received 3 August 2017, in final form 21 February 2018)

ABSTRACT

Coupled data assimilation is emerging as a target approach for Earth system prediction and reanalysis systems. Coupled data assimilation may be indeed able to minimize unbalanced air–sea initialization and maximize the intermedium propagation of observations. Here, we use a simplified framework where a global ocean general circulation model (NEMO) is coupled to an atmospheric boundary layer model [Cheap Atmospheric Mixed Layer (CheapAML)], which includes prognostic prediction of near-surface air temperature and moisture and allows for thermodynamic but not dynamic air–sea coupling. The control vector of an ocean variational data assimilation system is augmented to include 2-m atmospheric parameters. Cross-medium balances are formulated either through statistical cross covariances from monthly anomalies or through the application of linearized air–sea flux relationships derived from the tangent linear approximation of bulk formulas, which represents a novel solution to the coupled assimilation problem. As a proof of concept, the methodology is first applied to study the impact of in situ ocean observing networks on the near-surface atmospheric analyses and later to the complementary study of the impact of 2-m air observations on sea surface parameters, to assess benefits of strongly versus weakly coupled data assimilation. Several forecast experiments have been conducted for the period from June to December 2011. We find that especially after day 2 of the forecasts, strongly coupled data assimilation provides a beneficial impact, particularly in the tropical oceans. In most areas, the use of linearized air–sea balances outperforms the statistical relationships used, providing a motivation for implementing coupled tangent linear trajectories in four-dimensional variational data assimilation systems. Further impacts of strongly coupled data assimilation might be found by retuning the background error covariances.

[©] Supplemental information related to this paper is available at the Journals Online website: <https://doi.org/10.1175/MWR-D-17-0222.s1>.

^a Current affiliation: Centre for Maritime Research and Experimentation, NATO Science and Technology Organization, La Spezia, Italy.

Corresponding author: Andrea Storto, andrea.storto@cmcc.it, andrea.storto@cmre.nato.int

1. Introduction

Ingestion of observations in Earth system models through coupled data assimilation (DA) procedures is becoming the target strategy for initializing short- to long-term prediction systems and for climate reanalysis applications in many operational and research centers. Attention to coupled data assimilation challenges from the scientific community is also testified: for instance,

by the recent organization of a dedicated workshop sponsored by the World Meteorological Organization (WMO) World Weather Research Programme (WWRP) (Penny et al. 2017). At the national level, the Met Office has recently configured a coupled atmosphere–ocean short-range prediction system that implements a weakly coupled data assimilation strategy (Lea et al. 2015), that is, where the atmosphere and ocean data assimilation systems are independent but use coupled background fields, implying that a coupled atmosphere–ocean general circulation model (AOGCM) is used in the forecast step. The Japan Agency for Marine-Earth Science and Technology (JAMSTEC) has successfully implemented a coupled four-dimensional variational data assimilation (4DVAR) system, with adjustment of air–sea fluxes in the analysis scheme, for pentadal predictions (Mochizuki et al. 2016), providing satisfactory multiyear predictions in the extratropical North Pacific Ocean.

Reanalyses have also benefited from the introduction of coupled data assimilation: at the U.S. National Centers for Environmental Prediction (NCEP), a prototypical version of the Climate Forecast System Reanalysis (CFSR) has been produced with a weakly coupled data assimilation scheme (Saha et al. 2010). At the European Centre for Medium-Range Weather Forecasts (ECMWF), the first Earth system twentieth-century reanalysis [Coupled Earth System Reanalysis (CERA-20C)] has been produced with a 4DVAR scheme in the atmosphere and a 3DVAR scheme in the ocean. CERA-20C includes atmosphere–ocean coupled model trajectories in both the forecast step and the atmospheric 4DVAR outer loops (Laloyaux et al. 2016a).

The weakly coupled data assimilation approach has the obvious advantage of being promptly ready as soon as the two data assimilation systems for the ocean and the atmosphere are available and an AOGCM is used, although issues related to, for example, the assimilation frequency and time window length, the tuning of error covariances, and the representation of the diurnal cycle may be non-trivial to treat (e.g., Lea et al. 2015). Upgrading weakly coupled data assimilation schemes to fully strongly coupled ones, where an observation from one medium can impact the other medium within the analysis increments, has several potential advantages. First, the intermedium observation synergy and observation impact may alleviate observational deficiencies in a single medium, optimizing the exploitation of the different observing networks (e.g., Laloyaux et al. 2016b). Second, strongly coupled data assimilation may also alleviate initialization shocks typical of uncoupled or weakly coupled data assimilation systems (Mulholland et al. 2015) by providing cross-medium balanced analyses. In the context of climate reanalyses, Dee et al. (2014) argue that strongly coupled assimilation may

also improve the consistency and conservation of global transports: for instance, using additional constraints as those recently proposed by Takacs et al. (2016) for maintaining water balance.

There exist several methods that are being investigated to solve the coupled data assimilation problem, with large differences in complexity. Laloyaux et al. (2016a) include intermedium observation propagation that stems from the use of the 4DVAR outer loops (nonlinear model updates) with the fully coupled model in the CERA system. The use of multiple outer loops implies that upper-ocean observations affect the near-surface atmosphere and conversely for near-surface meteorological observations. This approach successfully shows slight improvements with respect to the system with uncoupled data assimilation. An obvious extension of this approach would be the use of coupled linear trajectories, namely, in the 4DVAR inner loops; these may, however, be technically and computationally demanding. Mimicking this extension in a simpler air–ocean coupled system is one of the main goals of the work presented in this article. Alternatively, Frolov et al. (2016) proposed the introduction of an interface solver that retains independent data assimilation systems while allowing for cross-medium covariances at the air–sea interface through shared interface analysis. Sugiura et al. (2008) implemented a coupled 4DVAR system that augments the data assimilation state vector with air–sea flux adjustment factors, thus allowing for the cross-fluid exchange of information.

Fully coupled data assimilation systems where the control vector is only one and includes both atmospheric and oceanic variables are under development at present (e.g., Ngodock et al. 2016). This represents a major long-term effort, due to the intrinsic complexity of coding the tangent linear and adjoint of a fully coupled Earth system model. To avoid the need for coding a tangent linear and adjoint model, the local ensemble tangent linear model (LETLM) was formulated by Frolov and Bishop (2016) and later implemented in a coupled data assimilation context by Bishop et al. (2017), with the advantage that the linear propagator and its adjoint are approximated by flow-dependent multivariate regression models calculated from an ensemble of realizations (perturbed coupled forecasts). This avoids the need for explicit coding of the tangent linear and adjoint version of the coupled forecast model at the price of running an ensemble of coupled model trajectories.

Idealized configurations (e.g., single-column models) provide encouraging results on their ability in limiting initialization imbalances, as shown by Smith et al. (2015). Different time scales in the ocean and atmosphere, however, are not easy to account for and may lead to different choices of the assimilation time window, depending on the objective of the data assimilation—whether for forecast or reanalysis applications

(Fowler and Lawless 2016). This also implies difficulties in the definition and estimation of background error air–sea cross covariances; Lu et al. (2015), for instance, propose using lagged covariances to account for the atmospheric errors leading the ocean ones and enhancing the cross-medium correlations.

In ensemble-based assimilation systems, the solution may be achieved through the use of purely statistical (cross) covariances derived from ensemble coupled model realizations (Zhang et al. 2007; Holt et al. 2011; Sluka et al. 2016), thus simplifying the coupled data assimilation problem to the optimal perturbation generation problem. Coupled ensemble data assimilation systems may, however, suffer from the need for a large ensemble size (Han et al. 2013), which may prevent their feasibility in operational forecasting systems.

Variational data assimilation relies on the tangent linear assumption for complex observation operators (3DVAR and 4DVAR) and for the model trajectory (4DVAR); that is, the observation and model operators are linearized around the background state, assuming that the assimilation window is short enough not to break the tangent linear assumption (Mahfouf 1999). Although this assumption may seem improper for strongly nonlinear processes (e.g., sea ice dynamics and thermodynamics, air–sea exchange processes, and moist physics), it has been successfully applied to a wide range of strongly nonlinear physics, such as deep convection (Stiller 2009), lightning parameterization (Lopez 2016), and moist physics in general (Janisková and Lopez 2013). It is therefore appealing to envisage strongly coupled data assimilation systems that embed tangent linear modeling of the air–sea flux exchanges, as proposed later in the present work.

In this work, we summarize the main outcomes of investigations performed at Centro Euro-Mediterraneo sui Cambiamenti Climatici (CMCC) in the frame of the EU FP7 project ERA-CLIM2 (Buizza et al. 2018). We aim to assess the feasibility of introducing linearized air–sea relationships for a strongly coupled data assimilation scheme that uses a full ocean general circulation model coupled to an atmospheric boundary layer model: that is, an intermediate complexity coupled model that allows for thermodynamic (and not dynamical) air–sea coupling. As a proof of concept, the analysis scheme is applied to the problem of assessing the impact of the in situ ocean and atmosphere observing networks on coupled short-range (up to 7 days) forecast skill scores. With this configuration, strongly coupled data assimilation is evaluated with respect to weakly coupled data assimilation for the two cases where either oceanic or atmospheric observations are assimilated. Experiments that simultaneously assimilate both observing networks are not performed so

as not to mix these two observation types in our coupled model, which has significantly different complexity for the oceanic and the atmospheric components.

The article is structured as follows: section 2 describes the ocean and atmospheric boundary layer model, the data assimilation system, and the air–sea balance operator (detailed in the appendixes). Section 3 presents the main results from idealized and real observing network experiments. Section 4 summarizes and discusses the main achievements.

2. Model and data assimilation system description

In this section, we first introduce and describe the configuration of the coupled air–sea modeling framework. Second, we detail the ocean data assimilation system along with the linearized air–sea balance operator.

a. Atmosphere and ocean modeling framework

1) OCEAN GENERAL CIRCULATION MODEL

The ocean model component is NEMO v3.4 (Madec et al. 1998) coupled with the LIM2 sea ice model (Fichefet and Morales Maqueda 1997) with elasto-visco-plastic rheology (Bouillon et al. 2009), implemented at the 1/2° resolution as in Storto et al. (2014), with 75 vertical levels and partial steps (Barnier et al. 2006). The thickness of the vertical layers ranges from about 1 m at the sea surface to about 204 m at the bottom. The horizontal grid is tripolar (Madec and Imbard 1996). There is a 2-hourly coupling frequency between the atmosphere and the ocean, which also corresponds to the coupling frequency between the ocean and the sea ice model.

2) ATMOSPHERIC BOUNDARY LAYER MODEL

An atmospheric boundary layer model called Cheap Atmospheric Mixed Layer (CheapAML; Deremble et al. 2013), developed at Florida State University, is coupled to NEMO in this study. CheapAML provides a prognostic formulation for the air temperature (T2M) and specific humidity (Q2M) at 2 m, implementing advective, diffusive, and thermodynamic processes that explain the air–sea heat and moisture exchanges. Transfer coefficients between the atmosphere and the ocean are calculated according to the CORE bulk formulas (Large and Yeager 2004). Here, CheapAML uses the time-varying atmospheric boundary layer height taken from ERA-Interim (Dee et al. 2011), which also provides the boundary layer wind vector at 3-hourly frequency and the downwelling shortwave radiation. The shortwave radiation is taken daily, and the analytic

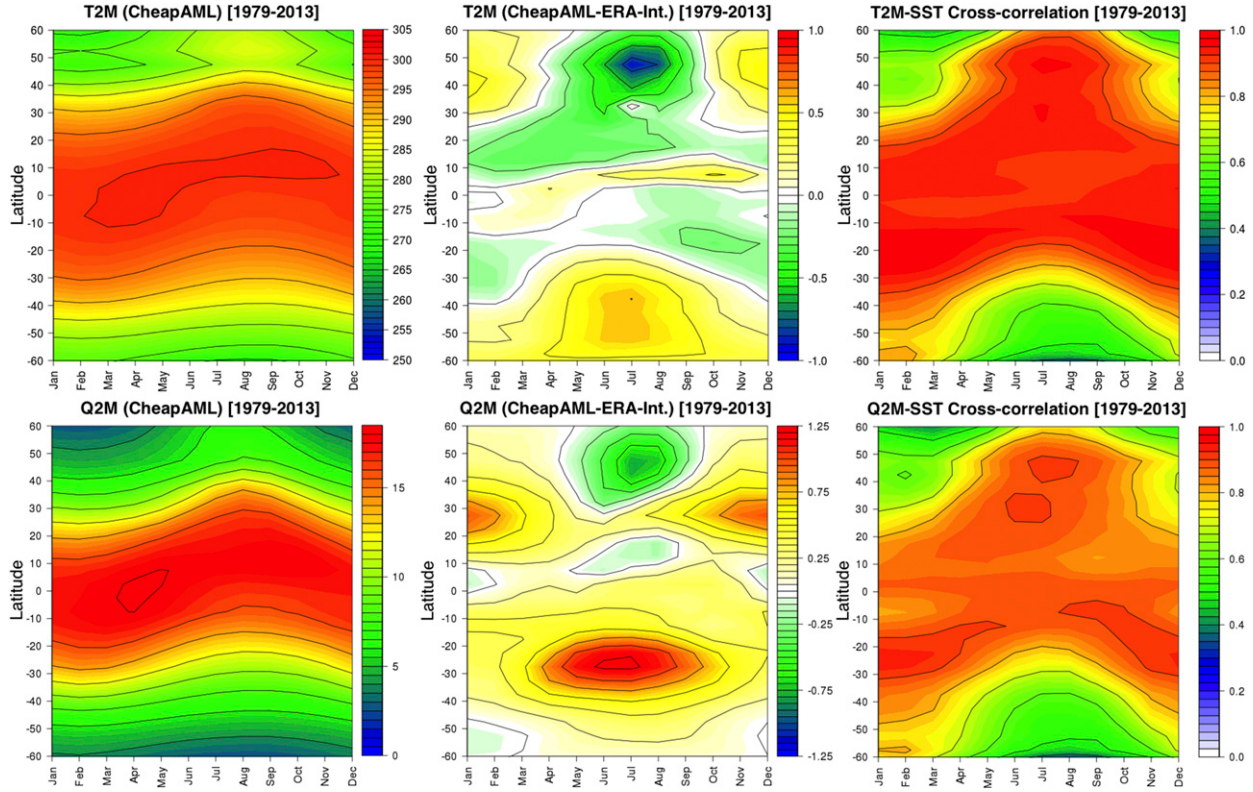


FIG. 1. (left) Long-term (1979–2013) climatology of 2-m air temperature (K) and specific humidity (g kg^{-1}), (middle) difference with respect to ERA-Interim, and (right) SST-T2M and SST-Q2M cross correlation for the NEMO–CheapAML ocean simulation.

diurnal modulation of [Bernie et al. \(2007\)](#) is used. Details of the CheapAML formulation and configuration are provided in [appendix A](#). Through the NEMO–CheapAML coupling, the assumption of infinite atmospheric heat capacity in forced ocean simulations is relaxed, and the air temperature is modified according to the exchange processes with the ocean, the parametric exchange with the free atmosphere, and advective and diffusive processes, thus implying two-way feedback between the ocean and the atmosphere, as in AOGCMs. However, the coupling is only thermodynamic and not dynamical; moreover, the coupled model is not free running, as the wind forcing, the atmospheric boundary layer height, and the incident shortwave radiative flux are provided by ERA-Interim, as in [Dereemble et al. \(2013\)](#).

The performance of CheapAML is evaluated in [Fig. 1](#) in terms of T2M climatology from a 1979–2013 NEMO–CheapAML simulation without data assimilation and compared to ERA-Interim analyses over oceans. The atmospheric boundary layer model is able to reproduce the large-scale features of near-surface air temperature. Biases with respect to ERA-Interim are generally small and below 0.5 K in the tropics (between 30°S and 30°N);

at higher latitudes, summer cold biases and winter warm biases occur, likely arising from the exchanges with the free atmosphere, the biases in the sea surface, and the uncertainties in the sensible heat flux estimates, and indicate an underestimation of the seasonal cycle of T2M by CheapAML. However, for the coupled assimilation experiments presented later, the CheapAML accuracy appears good enough. The top-right panel of [Fig. 1](#) reproduces the air-sea coupling in terms of T2M-SST cross correlation of monthly means over the period 1979–2013 from the simulation. At the monthly time scale, the coupling is strong in the equatorial region year-round and at midlatitudes during the summer season, when the ocean stratification is enhanced; conversely, during the winter season, characterized by deeper ocean convection, the same atmospheric thermal forcing produces smaller ocean temperature changes, resulting in a weak coupling between the sea surface and the near-surface atmosphere. However, this result may be affected by the neglect of the dynamical coupling in the NEMO–CheapAML coupled system, as extratropical regions are characterized by atmosphere-driving regimes ([Peña et al. 2003](#)), which here are neglected by

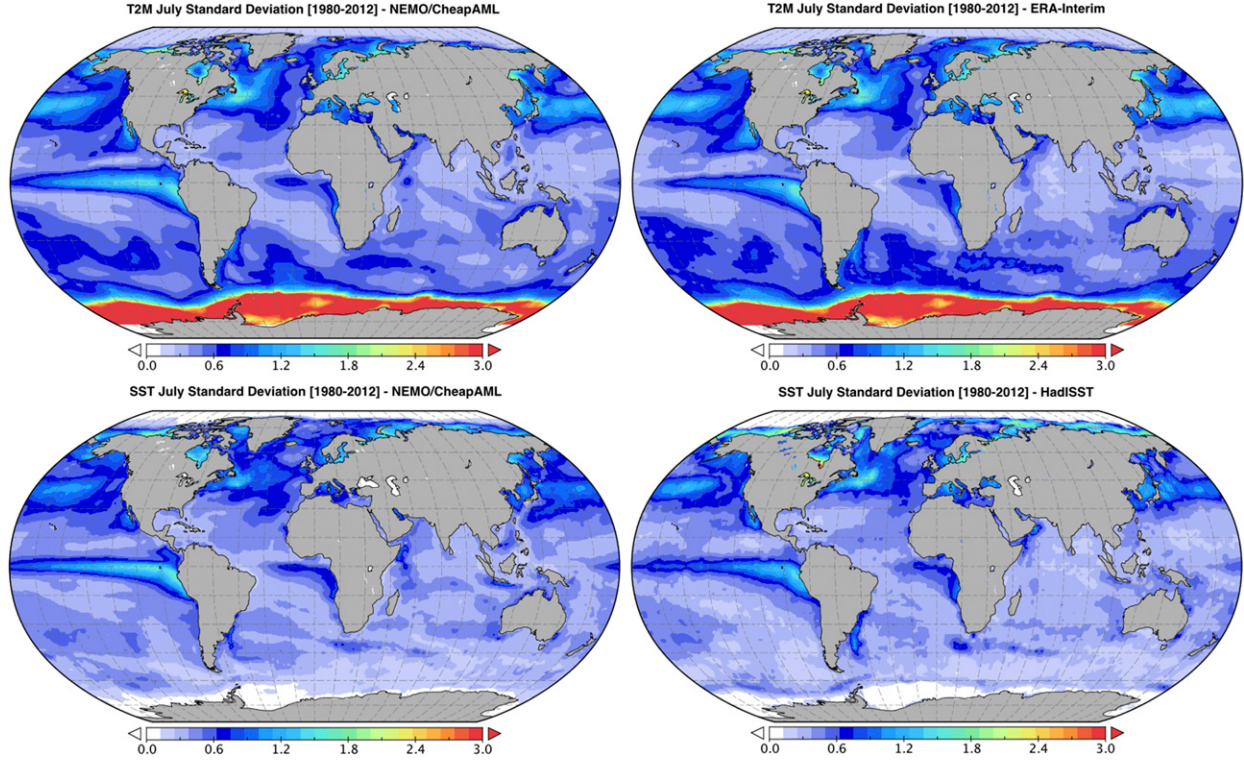


FIG. 2. July variability (standard deviation) over the period 1980–2012 for (top left) T2M and (bottom left) SST from the NEMO–CheapAML simulation and for (top right) T2M from ERA-Interim and (bottom right) SST from HadISST.

construction. In this regard, results shown in Fig. 1 are consistent with the ocean-driving regimes typical of tropical regions.

Similar results apply to the 2-m specific humidity (bottom panels of Fig. 1). The comparison against the ECMWF atmospheric reanalysis indicates a drier summer and wetter winter in CheapAML than ERA-Interim at high latitudes, although the biases are small, consistent with the T2M biases. The coupling between SST and Q2M exhibits qualitatively similar behavior to that between SST and T2M, although here, correlations are generally smaller than 1, even over the tropical region.

The July long-term variability of air and seawater temperature is shown in Fig. 2 and compared with ERA-Interim (Dee et al. 2011) for T2M and HadISST (Rayner et al. 2003) for SST. The variability of T2M in NEMO–CheapAML resembles that of SST, except around Antarctica, where, during austral wintertime, the T2M variability is affected by highly variable ice–ocean heat exchanges (especially sensible heat flux variability, not shown), while the SST exhibits low variability under sea ice. The T2M July standard deviation is reasonably close to that from ERA-Interim and, in turn, similar to the SST variability in HadISST,

suggesting that NEMO–CheapAML reproduces the interannual variability of T2M consistently with the atmospheric reanalysis data.

b. Formulation of OceanVar

The assimilation scheme is called OceanVar; it was originally developed for the Mediterranean Sea Forecasting System (Dobricic and Pinardi 2008) and later adapted to global ocean configurations (Storto et al. 2011), mostly for reanalysis applications (Storto et al. 2016; Storto and Masina 2016). The 3DVAR cost function is implemented in its incremental formulation (e.g., Courtier 1997), where $\delta\mathbf{x} = \mathbf{x} - \mathbf{x}^b$, with \mathbf{x} and \mathbf{x}^b being the state of the ocean and the background fields, respectively, and assuming one outer loop only. It reads:

$$J(\delta\mathbf{x}) = \frac{1}{2}(\mathbf{H}\delta\mathbf{x} - \mathbf{d})^T \mathbf{R}^{-1} (\mathbf{H}\delta\mathbf{x} - \mathbf{d}) + \frac{1}{2}\delta\mathbf{x}^T \mathbf{B}^{-1} \delta\mathbf{x}. \quad (1)$$

The tangent linear observation operator is \mathbf{H} [i.e., $\mathbf{H} = \partial\mathcal{H}(\mathbf{x})/\partial\mathbf{x}|_{\mathbf{x}^b}$], where $\mathcal{H}()$ is the observation function, mapping the ocean state in model space into observation space. Parameter $\mathbf{d} = \mathbf{y} - \mathcal{H}[\mathcal{M}(\mathbf{x}^b)]$ is the vector of misfits. Parameter $\mathcal{M}()$ is the model operator, used here to denote the first guess at appropriate time (FGAT) formulation; that is, misfits are evaluated by using model

equivalents at the same time of the observations. The terms \mathbf{B} and \mathbf{R} are the background and observation error covariance matrices, respectively. The analysis is defined as $\mathbf{x}^a = \mathbf{x}^b + \delta\mathbf{x}$ at the minimum of J .

The cost function formulation of Eq. (1) can be derived from Bayes' theorem, assuming Gaussian errors for the background and observations (Lorenc 1986) and neglecting the evolution of the ocean state within the assimilation time window.

The control variable transformation is used in OceanVar to precondition the minimization problem. The minimization is performed for the control variable \mathbf{v} , such that $\delta\mathbf{x} = \mathbf{V}\mathbf{v}$ with $\mathbf{B} = \mathbf{V}\mathbf{V}^T$.

Substituting, we obtain for the cost function

$$J(\mathbf{v}) = \frac{1}{2}(\mathbf{H}\mathbf{V}\mathbf{v} - \mathbf{d})^T \mathbf{R}^{-1} (\mathbf{H}\mathbf{V}\mathbf{v} - \mathbf{d}) + \frac{1}{2}\mathbf{v}^T \mathbf{v}. \quad (2)$$

The gradient of J is evaluated during the minimization for use with the limited-memory, quasi-Newton minimizer L-BFGS method (Byrd et al. 1995), and it is given by

$$\nabla J(\mathbf{v}) = \mathbf{V}^T \mathbf{H}^T \mathbf{R}^{-1} (\mathbf{H}\mathbf{V}\mathbf{v} - \mathbf{d}) + \mathbf{v}. \quad (3)$$

Modeling background error covariances is equivalent to applying the operator \mathbf{V} that is decomposed in a sequence of operators, assuming separability of the horizontal and vertical scales. In a general form, $\mathbf{V} = \mathbf{V}_b \mathbf{V}_h \mathbf{V}_v$. The vertical covariances operator \mathbf{V}_v is, in practice, modeled through multivariate empirical orthogonal functions (EOFs), namely, $\mathbf{V}_v = \mathbf{S}\Lambda^{1/2}$, where columns of \mathbf{S} contain multivariate eigenvectors, and Λ is a diagonal matrix with the corresponding eigenvalues.

Horizontal correlations (operator \mathbf{V}_h) are modeled through the application of a recursive filter. Here, we use a first-order recursive filter, although a third-order filter has been recently implemented (Farina et al. 2015). Periodic and shoreline boundary conditions are imposed with an artificial grid extension. The recursive filter coefficients depend on the model grid spacing and the correlation length scales, which can vary slowly in space (Storto et al. 2014; Mirouze and Storto 2016).

The operator \mathbf{V}_b controls the balances among the state variables and can take different forms, depending on the applications. For global applications, \mathbf{V}_b is the dynamic height balance converting increments of temperature and salinity into increments of sea level through local hydrostatic balance (Storto et al. 2011). While in uncoupled or weakly coupled data assimilation experiments the ocean state control vector \mathbf{x} includes only seawater temperature and salinity, in strongly coupled data assimilation experiments, it is augmented with 2-m air temperature and specific humidity; in this case, \mathbf{V}_b also embeds the analytic air-sea balances (see

section 2c). Alternatively, when balances are purely statistical—that is, implied by cross covariances between different parameters and implicitly contained in the multivariate EOFs operator \mathbf{V}_v (i.e., operator \mathbf{V} takes the simplest form $\mathbf{V} = \mathbf{V}_h \mathbf{V}_v$).

c. Air-sea balance operator for strongly coupled data assimilation

We introduce in this section the air-sea balance operator for use in strongly coupled data assimilation experiments. The operator is a tangent linear model that comes from the nonlinear thermodynamic processes embedded in the CORE bulk formulas (Large and Yeager 2004) and the CheapAML model (Deremble et al. 2013). Formally, the air-sea balance operator \mathbf{K}_a reads

$$(\delta T, \delta q) = \mathbf{K}_a(\delta T_o, \delta S); \quad (4)$$

namely, it returns increments of air temperature δT and humidity δq from increments of the sea state (with δT_o and δS as the ocean temperature and salinity increments, respectively). Its adjoint \mathbf{K}_a^T provides the back transformation. In OceanVar, it is part of the \mathbf{V}_b operator: after the control variable is transformed into profiles of temperature and salinity ($\mathbf{V}_v \mathbf{v}$) and the recursive filter correlates horizontally in space (\mathbf{V}_h), \mathbf{K}_a is applied to determine increments of air temperature and humidity. Formally,

$$\begin{aligned} (\delta T_o, \delta S) &= \mathbf{V}_h \mathbf{V}_v \mathbf{v}, \\ (\delta T, \delta q) &= \mathbf{K}_a^T \mathbf{V}_h \mathbf{V}_v \mathbf{v}, \quad \text{and,} \\ \delta \eta &= \mathbf{K}_d \mathbf{V}_h \mathbf{V}_v \mathbf{v} \end{aligned} \quad (5)$$

with $\delta \eta$ as the sea surface height increments and \mathbf{K}_d as the dynamic height operator (Storto et al. 2011). The detailed formulation of the air-sea balance operator is provided in appendix B. In this work, the transfer coefficients of evaporation and sensible heat, which depend on the atmospheric stability, are assumed not to depend on the ocean surface state and are taken from the nonlinear model trajectory because of the highly nonlinear iterative procedure for nonneutral coefficient computations of Large and Yeager (2004), although the fluxes in general are assumed to depend on the ocean state (see appendix B). In the future, this assumption may be relaxed. It is worth mentioning that the application of the air-sea balance operator mimics a coupled tangent linear model in a way that overcomes the problem of defining air-sea cross covariances through the tangent linear propagation (Smith et al. 2015). Given the fact that the operator is included in the definition of the background error covariance matrix and allows

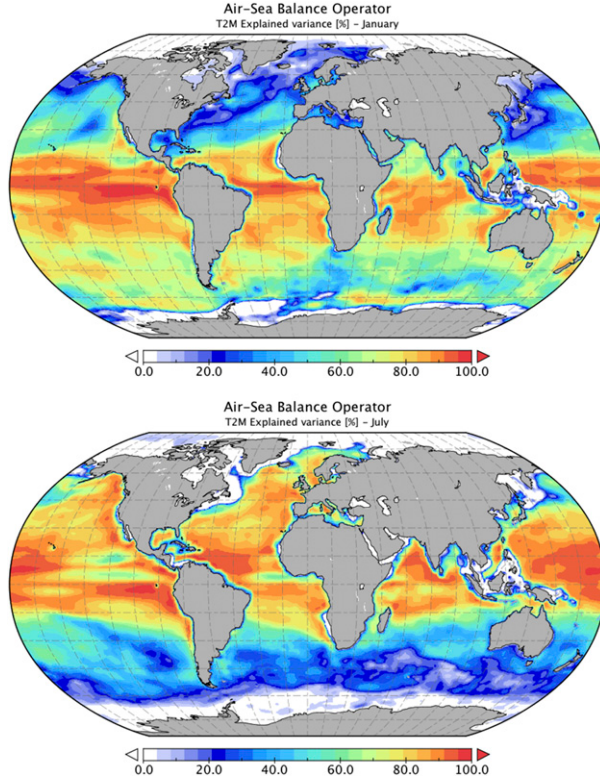


FIG. 3. T2M explained variance (EV; %) of the linearized air-sea balance operator with respect to the total variance, computed on monthly mean anomalies, for (top) January and (bottom) July. An EV of 100% means that the linearized air-sea balance operator explains all the variance. EV is defined as $EV = 100[\text{VAR}(x) - \text{VAR}(x - \hat{x})]/\text{VAR}(x)$, where x is the air-sea variable (either air temperature or humidity) from CheapAML, and \hat{x} is the one derived from ocean temperature through Eq. (5).

for cross-domain error covariances, its use lets our coupled data assimilation scheme fall into the strongly coupled data assimilation category, defined by Penny et al. (2017) as the one that treats the coupled system as one single integrated system and requires a cross-domain error covariance matrix be defined.

An insight into the performance of the air-sea balance operator is provided in Figs. 3 and 4, which show the T2M and Q2M explained variances of the operator with respect to the total variance, respectively, computed on monthly mean anomalies for January and July statistics. It appears that the operator proves able to explain the air-sea coupling (more than 70%) for the regions and seasons where the coupling is strong, (i.e., in the tropics and in summertime midlatitudes) and can be potentially applied to the strongly coupled data assimilation problem. Note that even if the balance operator is not seasonally dependent, strictly speaking, it is linearized around the time-varying background state and uses time-dependent SST perturbations; therefore, it

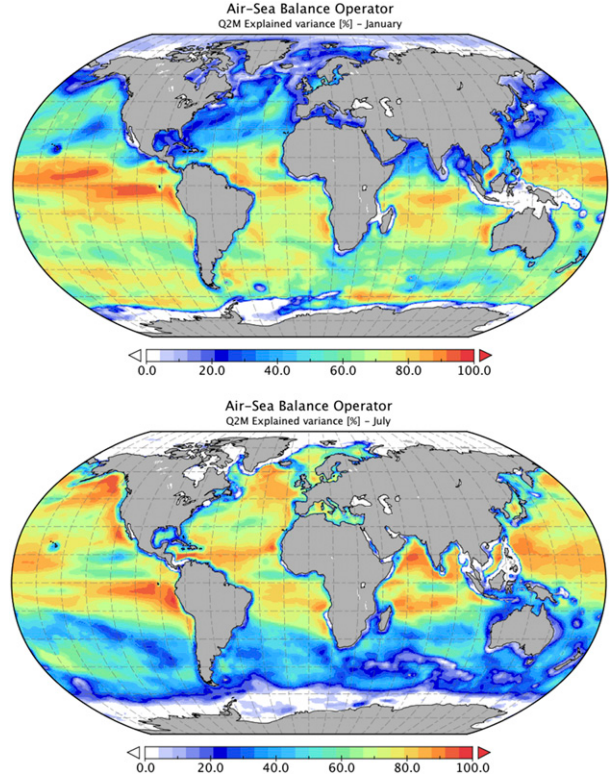


FIG. 4. As in Fig. 3, but for Q2M.

implicitly contains information on the seasonality. The operator proves more effective for T2M than for Q2M, in the sense that the explained variance is larger for T2M, although spatial patterns look very similar between the two variables.

d. Statistical balance operator for strongly coupled data assimilation

An alternative way for coupling atmospheric and oceanic parameters is by means of purely statistical covariances, as usually done in ensemble data assimilation systems (e.g., Sluka et al. 2016). In this case, we use a dataset of anomalies of T2M, Q2M, ocean temperature, and salinity to compute multivariate EOFs. Within this configuration, the vertical covariance operator directly provides air parameters in addition to ocean parameters:

$$(\delta T, \delta q, \delta T_o, \delta S) = \mathbf{V}_h \mathbf{V}_v \mathbf{v} \quad \text{and} \quad \delta \eta = \mathbf{K}_d \mathbf{V}_h \mathbf{V}_v \mathbf{v}, \quad (6)$$

and, formally, the operator \mathbf{K}_a reduces to the identity matrix.

To compute the statistical covariances, (i.e., the vertical EOFs), we extract monthly mean anomalies with respect to the long-term average from the 1979–2013 simulation presented in section 2a(2). EOFs are

calculated apart for each month of the year. In particular, we use the detrended monthly anomalies from the same month, the one before, and the one after, for a total of 35 years \times 3 months per each monthly EOF dataset. For each grid point, we use data from the 3×3 grid box centered on the grid point; this means that 945 profiles of perturbations are used for each EOF set over every grid point. We retain the first 20 leading EOFs that explain, on average, more than 95% of variance. When the air-sea balance operator of Eq. (5) is used, we used multivariate EOFs of ocean temperature and salinity; when Eq. (6) is used, multivariate EOFs of ocean temperature and salinity and air temperature and humidity were calculated and used, in either case taken from the same monthly anomaly dataset from the experiment in section 2a(2).

3. Experimental results

In this section, we present different experiments performed in order to evaluate the impact of strongly coupled data assimilation. In particular, section 3a presents results from a single ocean observation experiment performed with either weakly or strongly coupled data assimilation formulation; the propagation of the analysis increments on T2M is compared. In particular, we define weakly coupled data assimilation as the scheme where one observation contributes to analysis increments for parameters belonging only to the same medium as the observation (e.g., when ocean observations correct only ocean parameters), while strongly coupled data assimilation is when one observation corrects parameters also in the other medium (e.g., when ocean observations also correct atmospheric parameters), and the assimilation is applied to the atmosphere–ocean state simultaneously, treated as one single integrated system. Section 3b compares strongly versus weakly coupled data assimilation when ocean observations are assimilated, and verification skill scores are calculated for atmospheric parameters. Two different formulations of the air-sea balance for the case of strongly coupled data assimilation are also evaluated. Conversely, section 3c compares strongly versus weakly coupled data assimilation when atmospheric observations are assimilated and ocean verification skill scores are assessed. The comparison between weakly and strongly coupled data assimilation is performed independently for oceanic and atmospheric data assimilation in order to assess the impact of the observations from one medium on skill scores of the other medium without the effect of intramedium data assimilation.

a. Single-observation experiments

Single-observation assimilation experiments have been performed to assess differences between weakly and strongly coupled assimilation approaches. These allow us to understand, in a simplified framework, the intermedium propagation of the observational information by means of coupled data assimilation. In particular, the forecast model propagation of the 2-m air temperature analysis increments [$\mathcal{M}(\mathbf{x}^a) - \mathcal{M}(\mathbf{x}^b)$] is evaluated from the assimilation of a single observation of near-surface in situ seawater temperature in the tropical Pacific Ocean, simulating a single-level observation with an innovation (observation minus background) equal to 1 K. Figure 5 shows the results from an experiment in the tropical Pacific Ocean, where the forecast model propagation of the analysis increments is shown at +2, +12, +24, and +48 h since the analysis time for weakly coupled (left panels, no correction of 2-m air temperature in the analysis) and strongly coupled (right panels) configurations. Note that this is 2-hourly coupling, and the first air-sea heat flux exchange between NEMO and CheapAML occurs at initialization time. By construction, the propagated analysis increments of T2M are null at +0 h and practically zero at +2 h in the weakly coupled case, while they resemble the analysis increments coming from the air-sea balances in the strongly coupled case. During the forecast model integration, the initial analysis increments are shaped mostly by the advective and diffusive processes implied in the forecast model propagation. However, at time +12 h, the weakly coupled case exhibits increments arising from the air-sea exchanges in the forecast model, which are much smaller than in the strongly coupled case, the maximum of the propagated analysis increment being halved with respect to the strongly coupled case. At +24 h, the two cases appear very close, yet the weakly coupled case shows slightly smaller increments. Finally, after 48 h since analysis time, the two cases reproduce the same propagation of the analysis perturbation and are not discernible any longer, suggesting that possible imbalances caused by the uncoupled data assimilation may last up to 24 h and more. Figure S1 in the online supplemental material shows the SST minus T2M difference as a function of forecast range for the single-observation experiments (at observation location) and the implied sensible heat flux for both the weakly and strongly coupled data assimilation case. In the weakly coupled case, the large SST minus T2M difference is reduced over time and corresponds to a sensible heat flux transferring heat from the ocean to the atmospheric boundary layer; conversely, strongly coupled

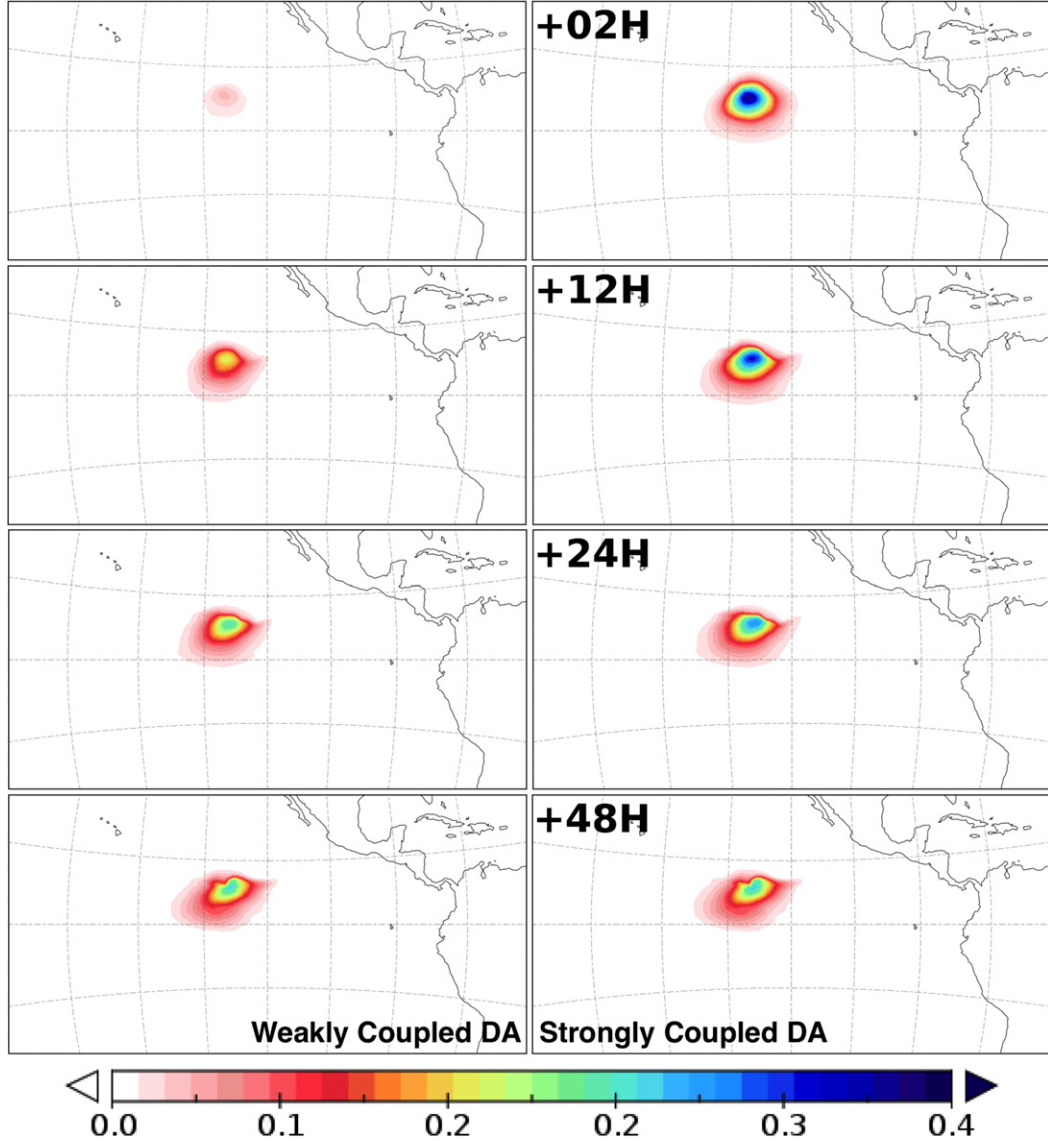


FIG. 5. Forecast model propagation of analysis increments (K) onto T2M increments at different forecast ranges for (left) weakly and (right) strongly coupled DA. The analysis increments come from single SST observation experiments, located at 7.5°N , 130.3°W .

data assimilation leads to almost neutral differences between SST and T2M (-0.04°C) that rapidly approach 0.07°C . The two coupling cases converge after about 40 h since analysis time.

To better quantify the weakly coupled data assimilation imbalance, Fig. 6 summarizes these diagnostics for summertime weakly and strongly coupled data assimilation experiments in the tropical Pacific Ocean (Figs. 6a,b), the Antarctic Circumpolar Current (ACC; Figs. 6c,d), and the Gulf Stream (Figs. 6e,f) regions, in terms of T2M (top panels) and sea surface temperature (SST; bottom panels) propagation, along with the percentage differences (dashed blue lines and right axes)

between weakly and strongly coupled cases. While differences in SST are not significant because the two cases assimilate the same observations in the ocean, differences between weakly and strongly coupled data assimilation greater than 10% last up to about 35 h in the tropics. Note that the 48-h value of T2M increments is smaller than the initial value in the strongly coupled data assimilation system; this might indicate overestimated cross covariances in the strongly coupled data assimilation case, although diffusive processes (in the upper ocean and in the atmospheric boundary layer) may contribute themselves to decrease the increments with time. In the ACC, the weak air-sea coupling in the

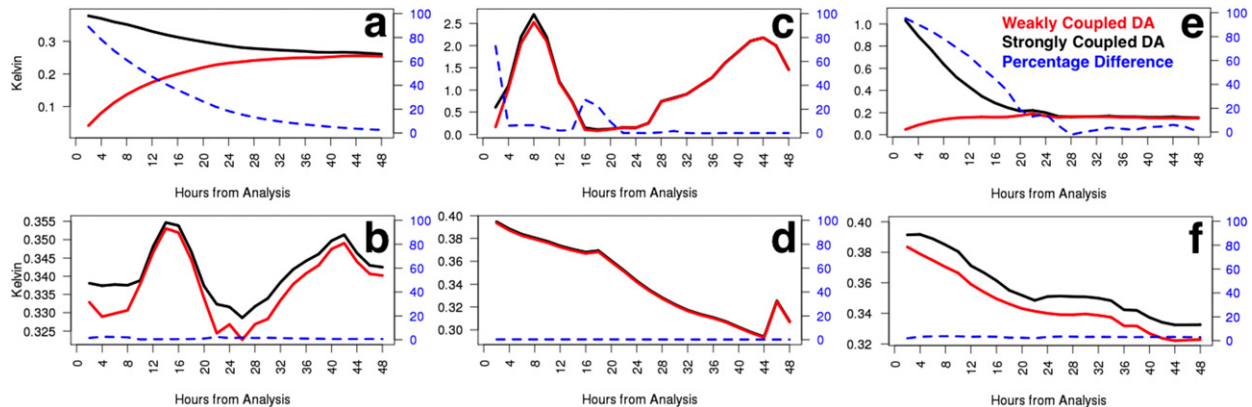


FIG. 6. Forecast model propagation of analysis increments (K) onto (top) T2M and (bottom) SST increments as a function of the forecast range in weakly (red lines) and strongly (black lines) coupled DA experiments. (a), (b) Tropical Pacific Ocean, (c), (d) the ACC, and (e), (f) the Gulf Stream regions, with test cases of observations located at 7.5°N , 130.3°W ; 57.0°S , 113.0°W ; and 42.0°N , 59.0°W , respectively. Blue lines refer to the percentage difference, which uses the blue axis on the right.

austral winter season leads to an imbalance that disappears quickly within the first 3 h since analysis time. Conversely, the strong coupling of the boreal summer in the Gulf Stream region leads to T2M imbalances greater than 10% for approximately the first 24 h. Such results confirm the potential advantages of the strongly coupled data assimilation, especially in the tropics and summertime midlatitudes and on short time scales; the latter is, in turn, important for short-range coupled forecasting and reanalysis applications. The dynamical coupling between marine winds and the upper ocean may provide qualitatively similar results due to the season-dependent upper-ocean structure, although this cannot be verified with the CheapAML atmospheric boundary layer model.

b. Real oceanic observing networks experiments

We present in this section results from real observing networks, where the main goal is to assess the impact of ocean observations on near-surface air parameters, evaluating the relative impact of both the linearized air-sea balance operator and a statistical operator.

1) CONFIGURATION

The experiments have been run for the 7-month period from 1 June to 31 December 2011. The list of experiments is reported in Table 1. All the experiments, except CTRL, consist of a daily assimilation cycle with a 1-day assimilation time window, followed by a 7-day forecast. During the 7-day forecast, the wind forcing is provided by ERA-Interim forecasts (provided by ECMWF) in order to mimic the decrease of wind accuracy with the forecast lead time. The experiments assimilate all hydrographic profiles from EN4 (Good et al. 2013) and along-track sea level anomaly data from

AVISO (Le Traon and Ogor 1998). The assimilation of SST is not included in the experiments in order to better observe the potential impact of the hydrographic profiles on the near-surface atmosphere and because the reanalysis system that experiments are based upon (Storto and Masina 2016) has not been extensively tested with satellite SST assimilation.

A nontrivial issue in coupled data assimilation is the choice of the assimilation frequency and time window, provided that the resolved ocean time scales are generally slower than the atmospheric ones (e.g., Lu et al. 2015). This factor is important not only in terms of the time scale of the processes implicitly resolved by the coupled data assimilation system, but also in terms of how many observations fall within each assimilation time window.

To qualitatively estimate the time scale of ocean and atmosphere errors, we have investigated the decorrelation time scale of the errors of sea surface temperature and 2-m temperature. To this end, errors are assumed to be represented by differences in two state-of-the-art SST datasets—the Operational SST and Sea Ice Analysis (OSTIA) system (Donlon et al. 2012) and the NOAA OIv2 (Reynolds et al. 2007) products—and two

TABLE 1. List of experiments performed.

Experiment name	Coupled assimilation method
CTRL	No assimilation
WEAK	Weakly coupled DA
STR-L	Strongly coupled DA Linearized ocean-atmosphere balance [Eq. (5)]
STR-S	Strongly coupled DA Statistical balance [Eq. (6)]

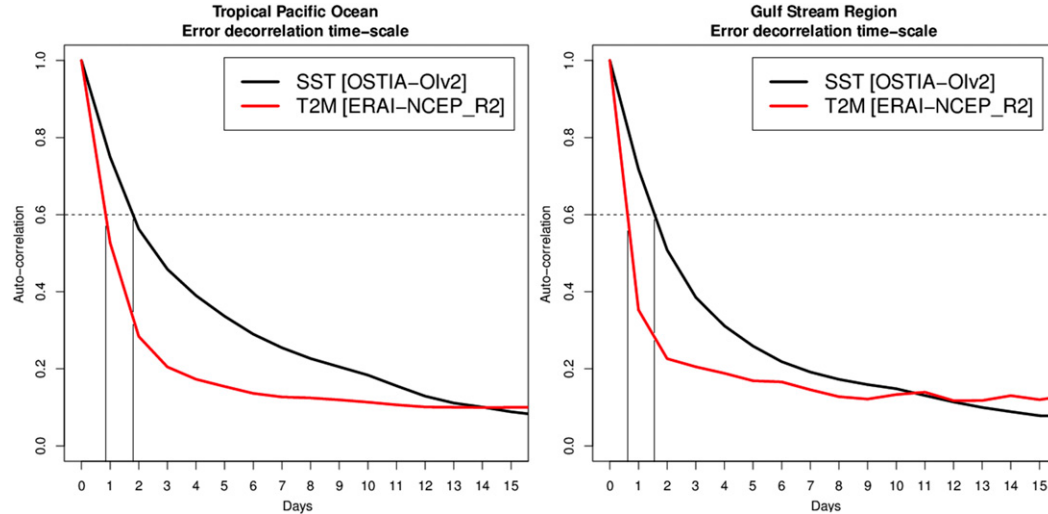


FIG. 7. Temporal decorrelation time scales of SST (black lines) and T2M (red lines) errors, estimated during 2011 from the difference of OSTIA minus NOAA OIv2 and ERA-Interim minus NCEP R2, respectively. (left) Tropical Pacific and (right) the Gulf Stream regions. The dashed lines correspond to the 0.6 autocorrelation value, while the thin vertical lines correspond to the time that matches the 0.6 correlation.

state-of-the-art atmospheric reanalyses—ERA-Interim (Dee et al. 2011) and the NCEP R2 (Kanamitsu et al. 2002). Differences were collected for the year 2011, and results are shown in Fig. 7 in terms of the temporal autocorrelation of the errors for the tropical Pacific Ocean and the Gulf Stream regions. No significant differences are found for the empirical error autocorrelation functions in the two regions. The Gulf Stream region exhibits a slightly shorter time scale, but for both areas, defining the decorrelation time scale as the time corresponding to 0.6 autocorrelation, the SST decorrelation time scale is approximately equal to 2 days, while that of 2-m air temperature is equal to 1 day; that is, the time scale of ocean temperature errors is roughly 2 times slower than that of the air temperature. From this sketch, we choose daily assimilation frequency and 1-day assimilation time windows as the minimum time during which both oceanic and atmospheric systems exhibit correlated errors. Note, however, that for climate-scale applications (e.g., Earth system reanalyses), more sophisticated approaches can be chosen, such as the lagged covariance method proposed by Lu et al. (2015). The nonlinear model trajectories used within STR-L (see Table 1) for the linearization of the air-sea balance operator are 6-hourly trajectories. Furthermore, the temperature and salinity background error covariances are the same in STR-L and STR-S for the sake of comparison. In STR-L, the T2M and Q2M covariances are implied by the application of the linearized air-sea operator, while in STR-S, they are statistical and included in the vertical multivariate EOFs.

2) IMPACT ON FORECAST ERRORS

In this section, we investigate the impact of strongly coupled data assimilation with respect to weakly coupled data assimilation in terms of forecast errors for the experiments presented above. In particular, we show skill scores for up to 7 days of forecast lead in order to assess the data assimilation schemes on realistic short- to medium-range forecasts, provided that results about forecast ranges longer than 7 days may be much too affected by the simplifications of the NEMO-CheapAML coupled model. Figure 8 compares the root-mean-square error (RMSE) of the forecasts calculated against all in situ observations of temperature and humidity at 2 m as a function of the forecast range and grouped for the tropical and extratropical oceans separately. These observations were extracted from the ECMWF operational archive. The verification of temperature in the tropics indicates that benefits of the strongly coupled data assimilation scheme emerge after day 2 of the forecast and increase up to day 7, although they remain small. In particular, especially for forecast ranges greater than 3 days, the use of linearized ocean-atmosphere balance relationships in STR-L outperforms the use of statistical covariances. We speculate that this is because the air-sea balance operator provides more balanced coupled initial conditions than the statistical operator. For the extratropical regions, differences of RMSE among the experiments are not significant. The RMSE scores for humidity show a similar behavior where differences are generally significant in

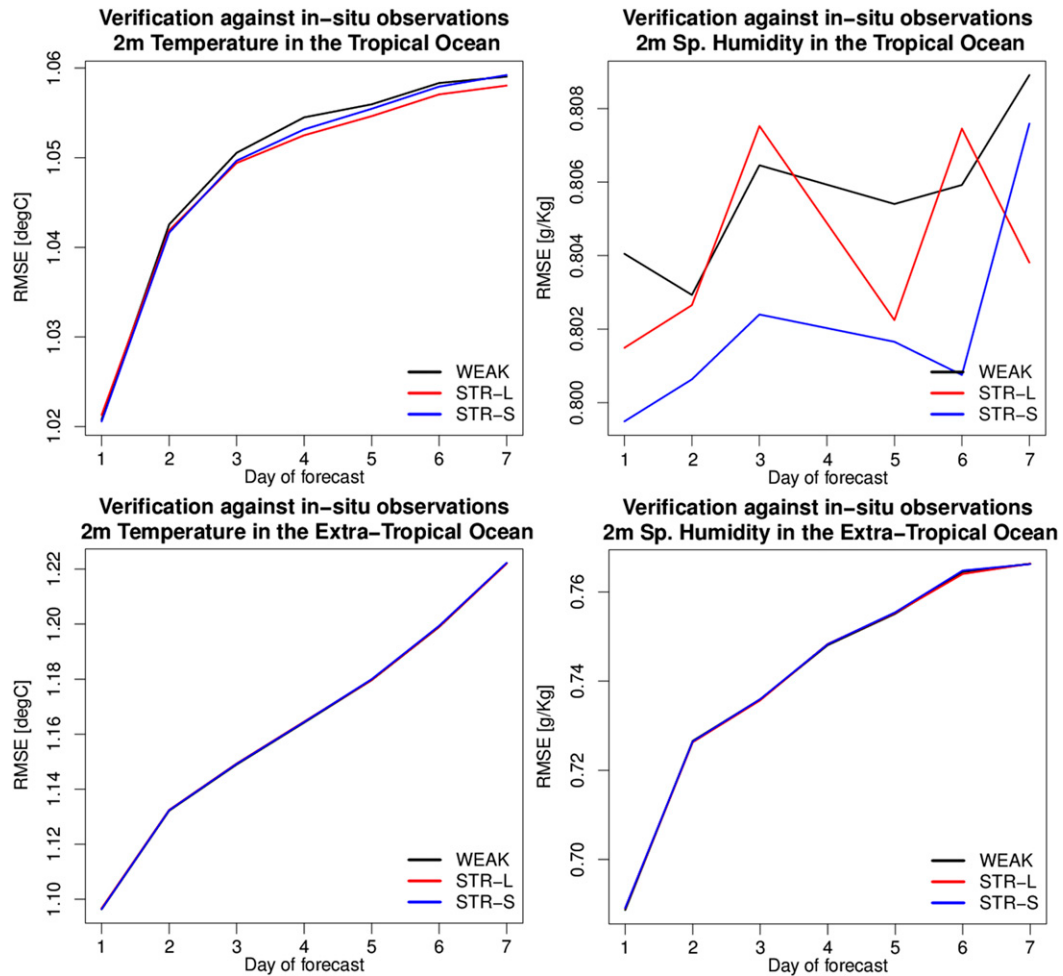


FIG. 8. RMSE of (left) T2M and (right) Q2M in the experiments described in the text against in situ observations for the (top) tropical and (bottom) extratropical oceans.

the tropical regions but not in the extratropical regions; strongly coupled DA appears to be providing smaller RMSE at all forecast ranges, where STR-S generally outperforms STR-L, except for the longest forecast ranges. Note also that for humidity, the increase of RMSE with forecast ranges in the tropics is somehow more irregular than for the temperature case, probably due to the relatively short experimental period and possibly because the simplified CheapAML model lacks a complete representation of moisture processes.

Given that most of the sensitivity in the choice of the coupled data assimilation scheme is found in the tropical regions and is likely related to the thermodynamic coupling used in this study, skill scores are now analyzed for the validation against tropical moorings: that is, the PIRATA, Research Moored Array for African–Asian–Australian Monsoon Analysis and Prediction (RAMA), and TAO arrays in the tropical Atlantic, Indian, and

Pacific Oceans, respectively (McPhaden et al. 1998). This is shown in Fig. 9 for 2-m temperature only. The RMSE differences are significant only in the Atlantic Ocean, based on a two-sample *t* test with a 90% confidence level. In this sector, the impact of strongly coupled data assimilation appears more significant, with a larger impact of the statistical formulation of the intermedium balances (with an RMSE decrease up to 4%, compared to the weakly coupled data assimilation configuration). In the other two sectors (Pacific and Indian Oceans), linearized balances provide the best skill scores for long forecast ranges (from day 3 of the forecast onward), although the impact is slightly smaller and statistically nonsignificant. Note also that in this comparison against moorings, weakly coupled DA appears more skillful in the first 2 days of the forecast, while less so afterward, suggesting that the increment borne by the strongly coupled DA

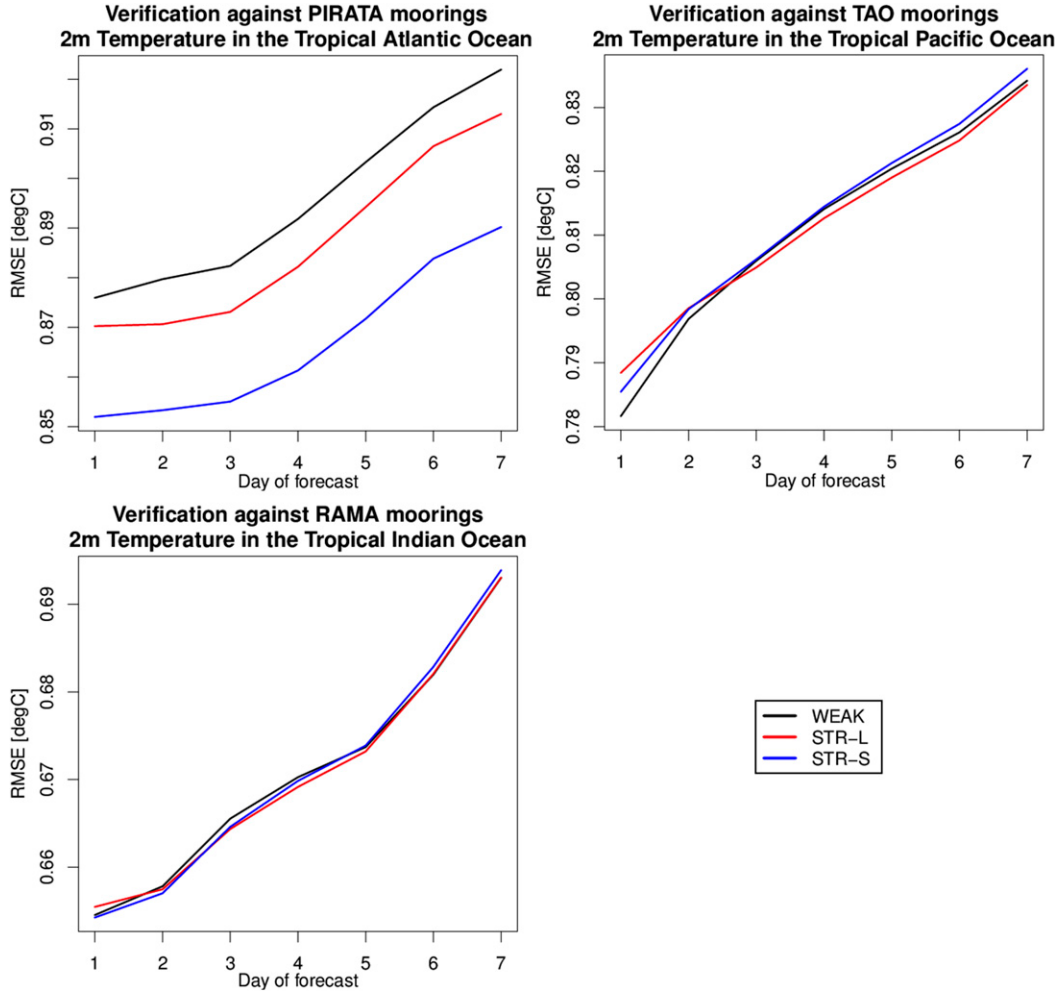


FIG. 9. RMSE of T2M in the experiments described in the text against observations from the tropical moorings in the (top left) Atlantic, (bottom left) Indian, and (top right) Pacific Oceans.

scheme, namely, the ocean–atmosphere cross correlations, may be correct but overestimated by both methods, and they are only effective after day 2 of the forecasts.

Figure 10 shows RMSE statistics as a function of the forecast range for Q2M, verified against the tropical moorings. The RMSE scores indicate that strongly coupled data assimilation is effective in the Atlantic Ocean (where RMSE reduction with respect to weakly coupled data assimilation is significant), with the best scores provided by STR-S. In the other tropical areas, while the impact is small and not significant, STR-L leads to the best score and slightly outperforms the weakly coupled data assimilation in both the tropical Indian and Pacific Oceans.

Figure 11 shows the map of RMSE increase or decrease for three pairs of experiments, calculated over the experimental period for the validation of 2-m

temperature at day 7 of the forecast against the tropical mooring data. The top panel shows the comparison between WEAK and STR-L experiments, indicating the positive impact of strongly coupled data assimilation in correspondence to many Pacific and most Atlantic buoys, although some buoys exhibit a detrimental impact. However, a small impact is found in the Indian Ocean, with significant improvement only in the eastern part of the domain due to the already high accuracy of the WEAK experiment in that region (not shown). In the Atlantic Ocean, the impact is neutral or positive everywhere, except for the mooring located in the Gulf of Guinea, whose result may be affected by a too-difficult representation of the freshwater-driven circulation (Storto 2016) and coastal processes. For this buoy, the statistical ocean–atmosphere relationships (STR-S) appear more appropriate (middle panel of Fig. 11), leading to a positive impact of strongly coupled DA. In

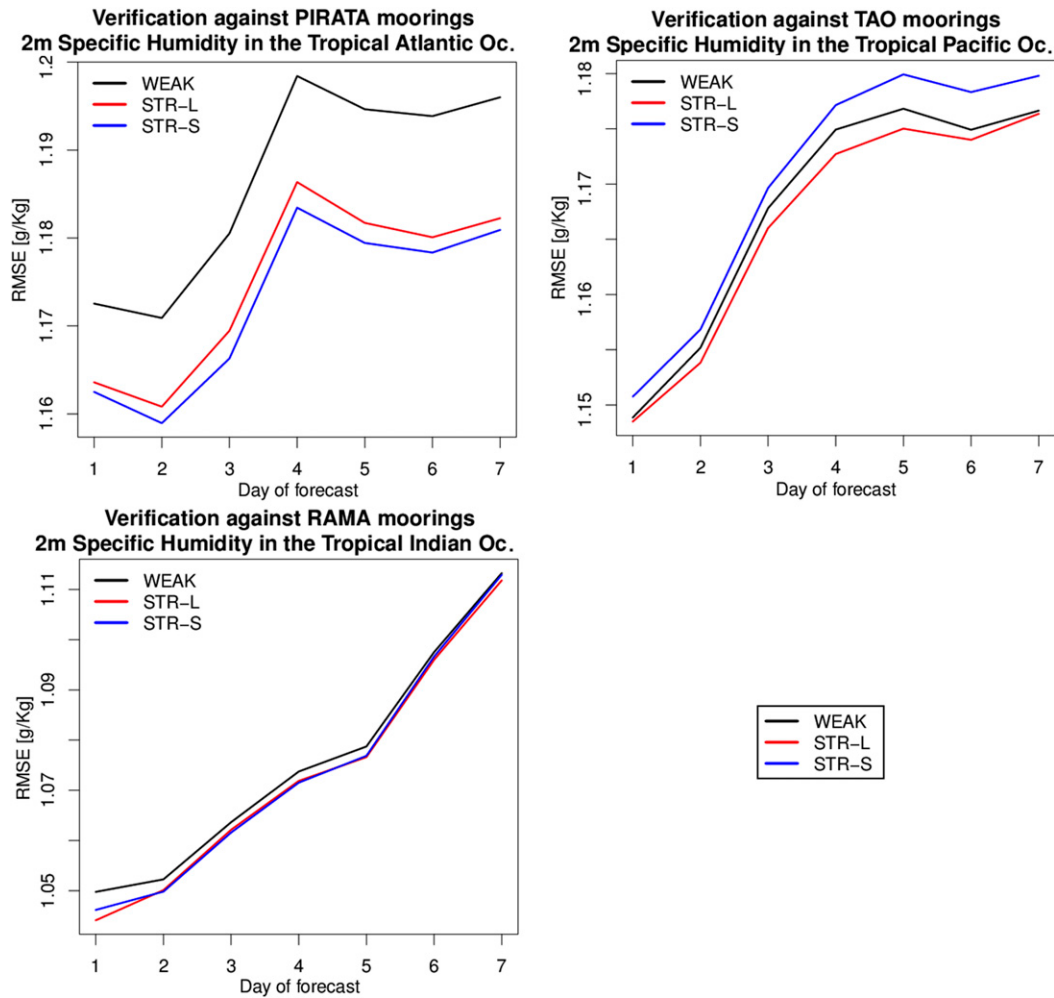


FIG. 10. As in Fig. 9, but for Q2M.

the Pacific Ocean, the impact of STR-L is overall positive, although there exist spots of detrimental impact of strongly coupled DA in the central western Pacific area (moorings located between 180° and 200°E), probably due to the high accuracy of the WEAK experiment (not shown) and because in this particular region, the variability of SST is larger than T2M in both observation- and model-based monthly mean data (see Fig. 2). The assimilation of ocean temperature data might consequently overestimate the corrections of T2M: for instance, if the errors assigned to the ocean temperature observations are underestimated. The STR-S experiment appears less skillful in the Pacific Ocean, with many moorings showing deterioration of the RMSE. This fact is also evident in the direct comparison between STR-L and STR-S (bottom panel of Fig. 11). While the recourse to statistical balances appears important in the tropical Atlantic Ocean, the Pacific Ocean shows a clear improvement when linearized balances are

adopted, suggesting that the optimal choice may depend on local regimes, and covariances may require further tuning. In the equatorial Atlantic Ocean, as well as in a few equatorial buoys in the Pacific Ocean, STR-S outperforms STR-L, likely due to the high variability of heat fluxes (Fig. 13) that might be damped out by the approximated linearization implicit in the use of STR-L.

Finally, we verify the impact of the coupling strategies on oceanic verification skill scores; see Fig. S2, which shows the time series of root-mean-square error in the top 5 m against oceanic in situ measurements of temperature and salinity. RMSE does not vary significantly across the experiments, indicating that the coupling strategy does not affect the skill scores in the medium where observations are assimilated.

3) IMPACT ON BIASES AND AIR–SEA FLUXES

We now evaluate the effect of the coupled data assimilation strategy on the long-term (7-month period)

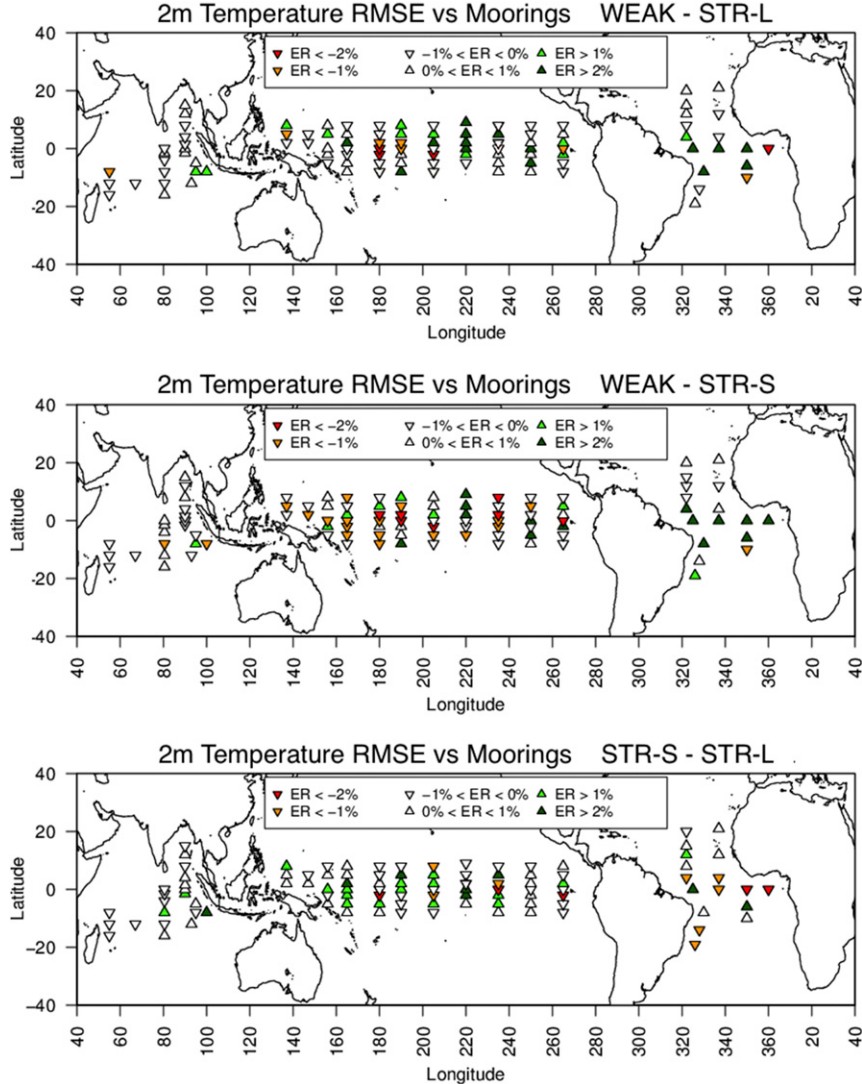


FIG. 11. Percentage error reduction (i.e., normalized RMSE difference) between pairs of experiments at forecast day 7 against observations from the tropical moorings. Positive (negative) error reduction indicates that STR-L, STR-S, and STR-L outperform (underperform) WEAK, WEAK, and STR-S in the three panels from top to bottom, respectively. Each triangle corresponds to a tropical mooring location.

biases of the experiments, evaluated against ERA-Interim. Although ERA-Interim is not a verification dataset per se, its use as a reference dataset may still help in understanding the differences among the experiments. Long-term means are calculated as the average of fields during the first day of the forecasts.

Figure 12 shows the 7-month biases of temperature (Figs. 12a,c,e) and humidity (Figs. 12b,d,f) at 2 m of the CTRL and WEAK experiments against ERA-Interim. Figures 12e and 12f also show the 7-month difference between STR-L and WEAK. During this period, the experiments are warmer (up to 3°C) than ERA-Interim in the Southern Hemisphere, in particular in the ACC,

in the South Atlantic Ocean, and in correspondence to the eastern upwelling regions of the Pacific and Atlantic Oceans and in the western Pacific warm pool. In the Northern Hemisphere, biases are smaller, both negative and positive, and never exceed 1°C. The weakly coupled data assimilation is able to reduce the warm biases in many areas, particularly in the Southern Ocean. Note that ERA-Interim uses SST analyses from satellite data as boundary conditions and does not include the assimilation of temperature or humidity at 2 m over sea; on the contrary, the ocean data assimilation system does not include the assimilation of satellite SST data. Thus, the decrease in the differences indicates that the ocean

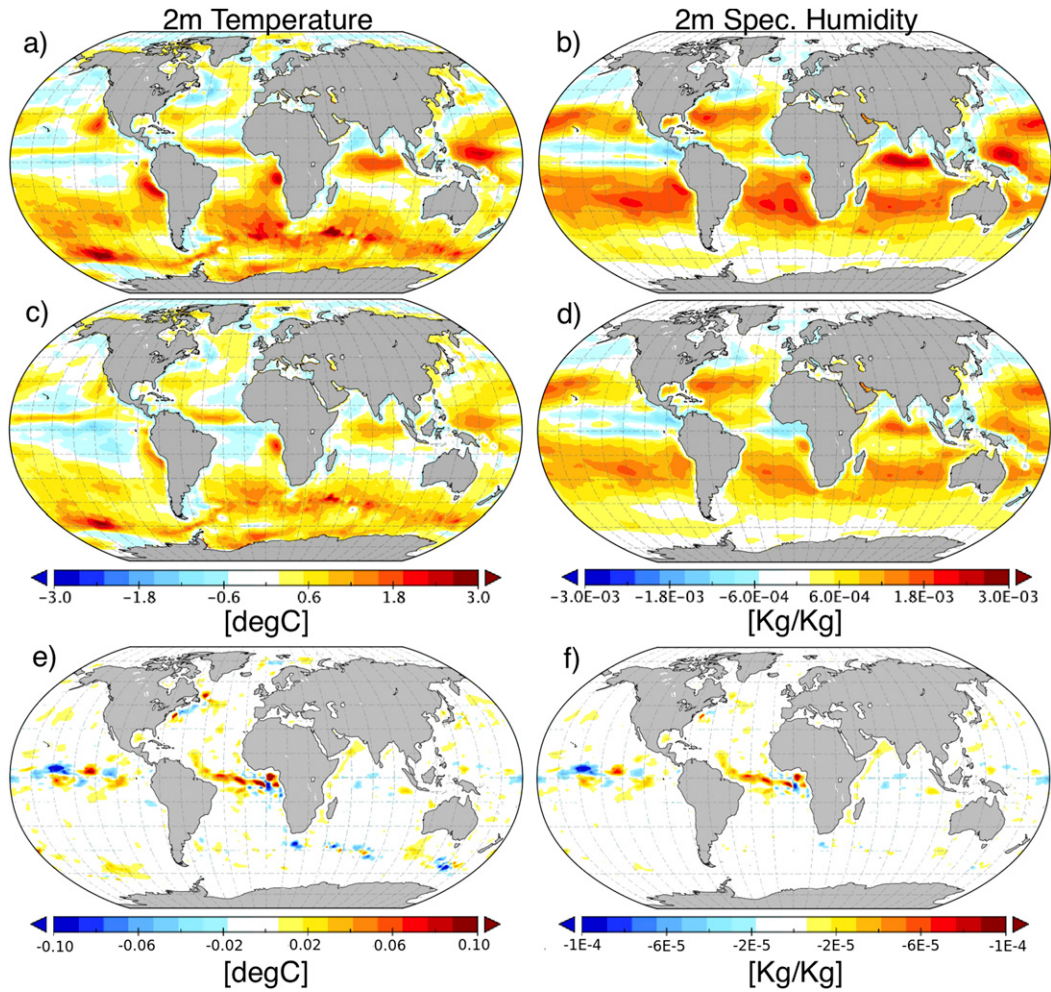


FIG. 12. The 7-month biases (from June to December 2011) of (a),(b) CTRL and (c),(d) WEAK, compared to ERA-Interim, and (e),(f) differences between STR-L and WEAK for (left) T2M and (right) Q2M.

in situ network is able to partly recover from the lack of SST data in terms of air temperature biases. However, the recourse to strongly coupled data assimilation does not further reduce the biases; differences between weakly and strongly coupled biases are not significant, suggesting that there is no impact of strongly coupled data assimilation on seasonal to yearly averages with our experimental configuration. The impact of different air-sea balance approaches (i.e., STR-L vs STR-S) on the bias is also not significant (not shown).

Similar considerations can be drawn for humidity biases, shown in the right panels of Fig. 12. The main wet biases occur at midlatitudes in both hemispheres. The weakly coupled data assimilation significantly reduces the biases at midlatitudes, although the strongly coupled data assimilation method, with either air-sea balance formulation, does not further reduce the biases. This result may be ascribed to the relatively long daily

assimilation time window, compared to the typical length used in atmospheric data assimilation systems, which may hide the impact of strongly coupled data assimilation. Indeed, most of the impact of marine observations on near-surface air parameters is already transferred by weakly coupled data assimilation during the 24-h time window.

Figures 13a and 13b show a zoom in the tropics, in particular where the 7-month mean differences between STR-L and WEAK are compared. The impact of strongly coupled DA is not large, peaking up to 0.3°C in the middle of the tropical Pacific Ocean and in the Gulf of Guinea in the Atlantic sector. Differences show small-scale variability rather than large-scale signals, suggesting local thermodynamic adjustments caused by the strongly coupled DA formulation. Differences in SST are slightly damped out in T2M, although they exhibit the same spatial patterns, implying that the effect

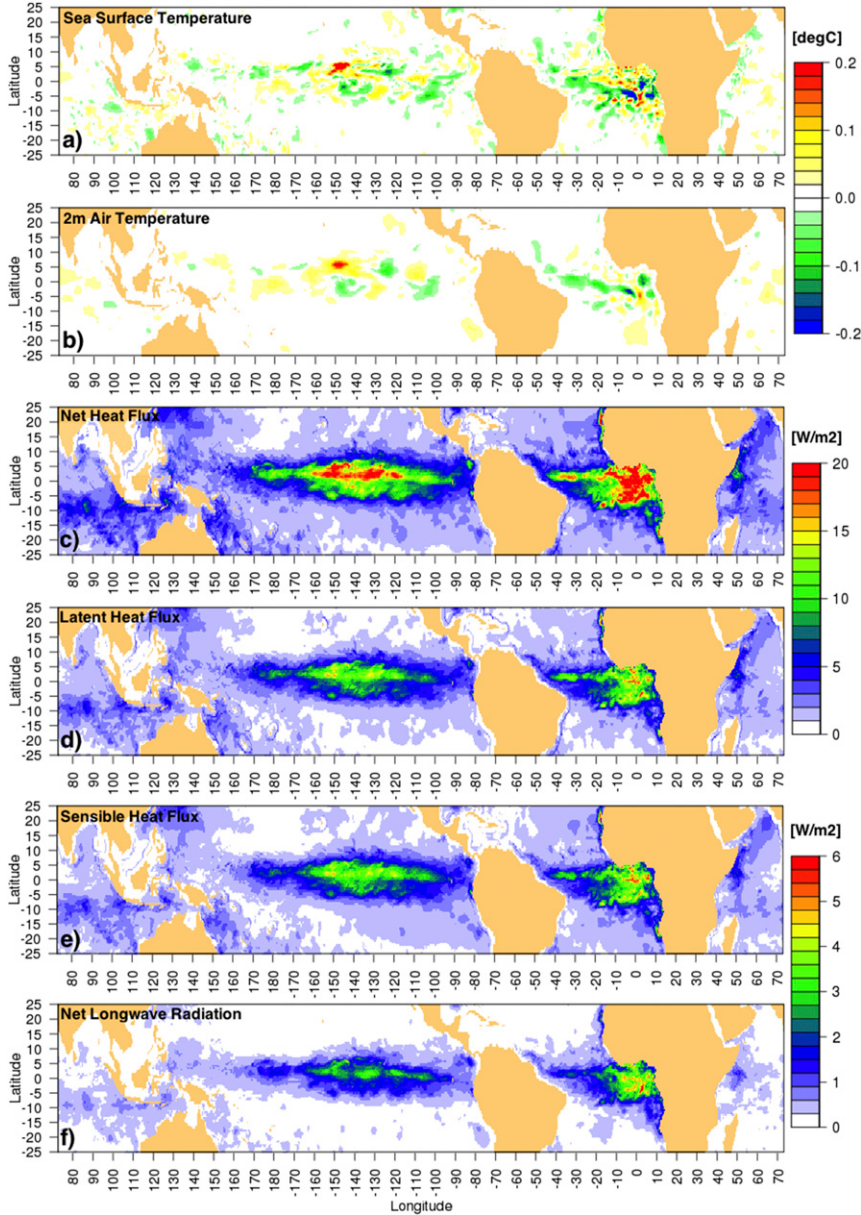


FIG. 13. In 2011 (from June to December), the average difference of (a) SST and (b) T2M between STR-L and WEAK in the tropics; standard deviation (W m^{-2}) of daily mean differences between STR-L and WEAK from June to December 2011 for (c) net heat flux, (d) latent heat flux, (e) sensible heat flux, and (f) net longwave radiation. Note that (e) and (f) have a different color scale than (c) and (d).

on air parameters is slightly smoother than that on the sea surface.

Figures 13c–f show the standard deviation of the air-sea heat flux component differences between STR-L and WEAK, thus providing a quantitative picture of the impact of the strongly coupled DA formulation on the heat fluxes' variability. Net heat fluxes show large variability (up to 20 W m^{-2}) in the middle of the Pacific Ocean and in the Atlantic Ocean equatorial band,

peaking in the Gulf of Guinea, consistent with the T2M and SST differences outlined previously. The largest contribution to the net heat flux variability between the two experiments comes from the latent heat flux. It should, however, be noted that in the CheapAML formulation, the latent heat is assumed to transfer directly above the atmospheric boundary layer (see also [appendices A](#) and [B](#)); namely, it does not directly contribute to the SST-T2M heat exchanges. This suggests

that in fully three-dimensional coupled AOGCMs, the impact of the strongly coupled data assimilation may be larger than that found with CheapAML, and coupled data assimilation may lead to different exchanges between the ocean and atmosphere, especially in low-latitude areas dominated by evaporative fluxes. Among the other flux components, sensible heat flux variability is larger than the net longwave radiation, with the shortwave radiation being the same in the two experiments. Although regions of maximum variability of differences are the same as the net heat flux, as they all rely on differences of SST and T2M among the experiments, the standard deviation is smaller (peaking at about 5 W m^{-2}). As the atmospheric boundary layer model does not include dynamical components, sensible heat differences respond directly to the SST minus T2M differences in each experiment, meaning that this estimate might be underestimated with respect to real-world cases. In summary, our configuration implements thermodynamic heat exchanges between air and sea, but the lack of atmospheric dynamics and moist physics might damp out the impact of strongly coupled data assimilation.

c. Real atmospheric observing networks experiments

Finally, we evaluate the impact of the strongly coupled data assimilation scheme for the case where only 2-m atmospheric observations are assimilated, and upper-ocean parameters' skill scores are evaluated for different configurations of data assimilation. Such experiments represent the complementary exercise to that of the previous section, where the lack of ocean observations is recovered through strongly coupled data assimilation of air parameters and are conceived to assess the potential of the atmospheric observations to correct the sea surface state in coupled analyses and forecasts. In particular, weakly coupled data assimilation (WEAK) is compared with strongly coupled data assimilation, with either analytic (STR-L) or statistical (STR-S) air-sea balance. To better appreciate the impact of the atmospheric observing network on ocean skill scores, ocean observations are not assimilated in these experiments; that is, the only difference in the results is due to the different formulation of the air-sea coupling and the assimilation of atmospheric observations. When the linearized air-sea balance operator is used, increments arising from the atmospheric observations are spread onto ocean variables through the adjoint of the operator [adjoint of Eqs. (B3) and (B4) in appendix B], while the use of the statistical operator implies that multivariate EOFs lead the observational spread between atmospheric observations and ocean parameters. As the salinity does not enter the linearized

air-sea balance operator (appendix B), differences in salinity among the experiments stem indirectly from the differences in temperature rather than from the data assimilation increments themselves. Statistical balances may, however, contain empirical correlations between salinity and air temperature or humidity, inferred from surface processes.

Here, we assimilate all available observations of T2M and Q2M from ships [synoptic (SYNOP SHIP); temperature, salinity, and current (TESAC); and bathythermographs (BATHY)] and drifting buoys (DRIBU), extracted from the ECMWF operational archive. Experiments were conducted in the same way as presented in section 3b(1), namely, a 7-month period from June to December 2011 with daily frequency of assimilation, each of them followed by 7-day forecasts. The Ocean-Var data assimilation system was modified to support the assimilation of T2M and Q2M. For this exercise, we set observational error for atmospheric observations independent of the geographical location and instrument type and equal to 0.75 K and 0.55 g kg^{-1} for temperature and specific humidity observations, respectively.

Similar to the case of the oceanic observing system experiments, we do not find significant differences in the mean state of the ocean (not shown), suggesting the small impact of the data assimilation coupling on the long-term means. Figure 14 shows the time series of the RMSE of temperature and salinity forecasts (from 5 to 7 days) calculated against independent near-surface ocean in situ observations (all available observations in the top 5 m of depth). Note that root-mean-square errors are relatively large due to the lack of any ocean observational constraint (neither in the data assimilation nor in the ocean model). The results indicate the small impact of the strongly coupled data assimilation in the extratropics, except for a number of selected cases—August in the southern extratropics and September in the northern extratropics, the latter visible only on salinity—where strongly coupled data assimilation performs slightly better than weakly coupled data assimilation. Tropical temperature skill scores show, however, a significantly positive impact of strongly coupled data assimilation with the linearized air-sea operator, especially during the first 4 months of the experiments. Also, statistical air-sea relationships provide slight improvements with respect to weakly coupled data assimilation.

Salinity skill scores (right panels of Fig. 14) show more complex behavior and a pronounced seasonal dependence (e.g., RMSE peaking in September in the northern extratropics). Except for a sudden increase of RMSE in the southern extratropics around August, the

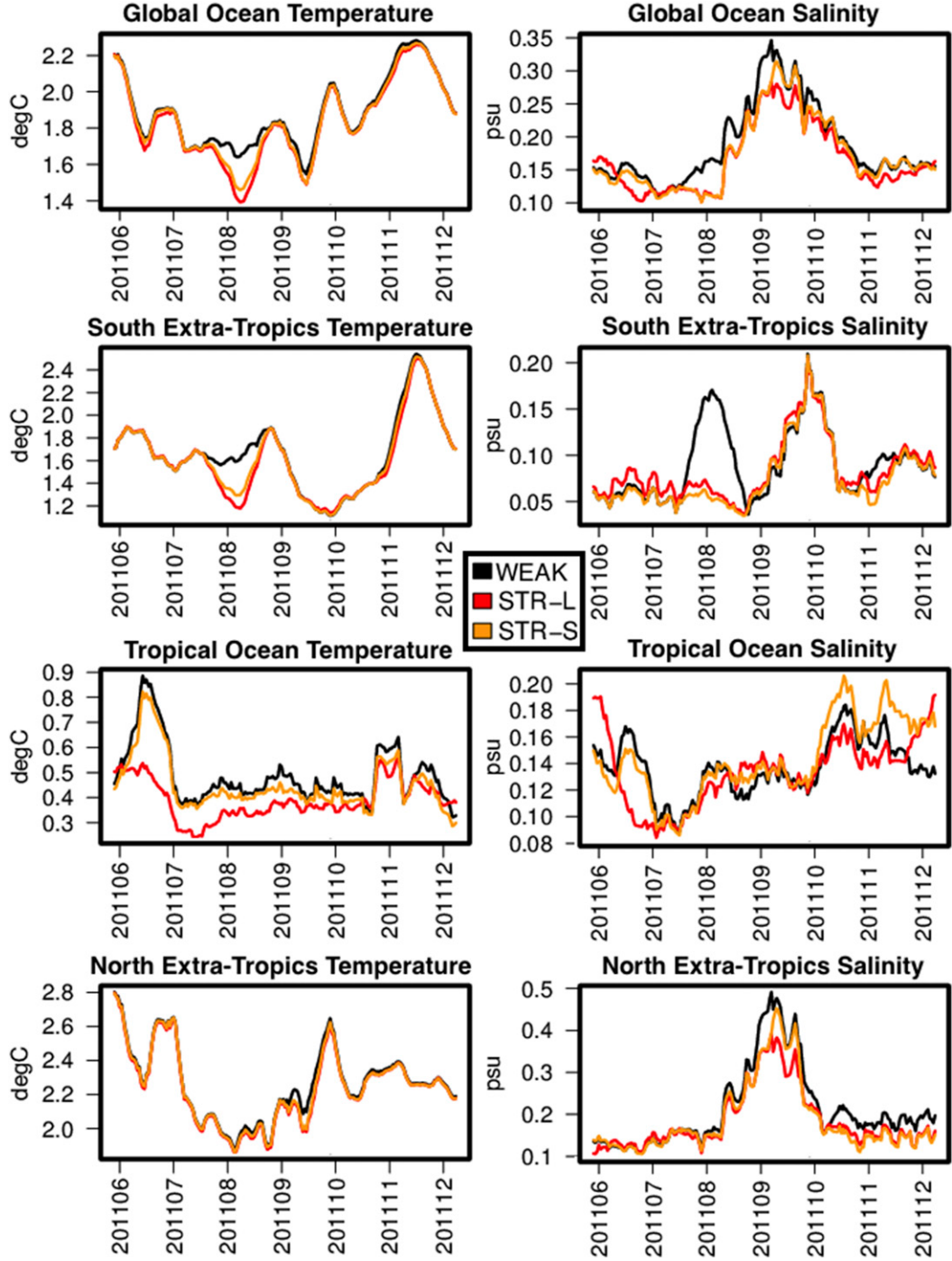


FIG. 14. Time series of RMSE of 5–7-day forecasts against near-surface (top 5 m) temperature ($^{\circ}\text{C}$) and salinity (psu) observations from the experiments WEAK, STR-S, and STR-L described in the text for the global ocean, the southern (90° – 30° S) and the northern (30° – 90° N) extratropics, and the tropics (30° S– 30° N). A 7-day running mean is applied to the daily statistics. All the observations are used, regardless of their instrument type.

impact of the data assimilation strategy is not significant, even in the tropics, consistent with the indirect impact of atmospheric observations on salinity through the seawater temperature.

To summarize, experiments performed by assimilating atmospheric observations in coupled data assimilation systems confirm that our configuration exhibits significant impact only in the tropical areas, where

strongly coupled data assimilation performed with the linearized air-sea balance operator provides the best skill scores, compared to the other data assimilation schemes.

Finally, Fig. S3 shows the verification skill scores of the three experiments against atmospheric observations, (i.e., as in Fig. 8, but for the experiments assimilating atmospheric observations). Similar to the case when oceanic observations are assimilated, RMSE does not vary significantly across the experiments, and the coupling method does not impact the medium where observations are already assimilated.

4. Summary and discussion

Here, we document strongly coupled data assimilation experiments performed with a simplified coupled model, where an ocean general circulation model is coupled with a one-layer atmospheric boundary layer model. There are several advantages of this approach. First, we avoid the use of a 3D atmospheric model that, in turn, would need the coupling between the oceanic and atmospheric data assimilation systems in order to perform strongly coupled data assimilation experiments. This would be technically and computationally demanding, although it represents the long-term objective of many operational forecasting centers. With our approach, we are able to modify the ocean data assimilation system and augment the ocean control vector to include the atmospheric boundary layer variables: that is, bypassing the need of a data assimilation coupler and/or interpolation procedures from/to oceanic and atmospheric computational grids, the latter defined in spectral space in most global atmospheric general circulation models. Second, the atmospheric boundary layer can be reasonably assumed to be the vertical region of the atmosphere where assimilating ocean observations may provide a beneficial impact. For instance, [Frolov et al. \(2016\)](#) developed a coupled data assimilation scheme based on the fundamental assumption that oceanic observations may impact the atmosphere only in the boundary layer, while atmospheric observations may impact the ocean only in the mixed layer. While the strategy of using an atmospheric boundary layer has all of these scientific and technical advantages, it cannot be used for a cross-medium impact of observations of wind or currents that may lead to improved representation of the surface temperature ([Laloyaux et al. 2016b](#)) because it allows for thermodynamic coupling only (and not dynamical). Consequently, we focus our investigations especially on the cross-medium impact of temperature observations (i.e., linked to air-sea heat exchanges). Indeed, it should be noted that the coupled NEMO-CheapAML model is

not free running, strictly speaking, as it inherits the wind forcing from external datasets—ERA-Interim in our case. The lack of atmospheric dynamics might also decrease the potential impact of strongly coupled data assimilation by partly damping out heat flux increments implied by the cross-medium balances.

Further limitations of the present studies consist of the use of background error covariances in the data assimilation system that come from monthly anomalies: that is, bearing error information at a time scale that is longer than that investigated in the experiments, where we compare medium-range forecast skill scores, as detailed later. The limited extension of the experimental period also prevents the significant impact of the coupled data assimilation techniques on interannual scales typical of climate applications (e.g., Earth system reanalyses).

The coupled NEMO-CheapAML model proves able to represent most of the temperature and humidity large-scale features. In particular, its bias with respect to, for example, atmospheric reanalyses such as ERA-Interim, is small, especially in the tropical region, and the interannual variability is close to that of the atmospheric reanalysis dataset. The study of air-sea temperature cross correlations indicates the strong coupling between ocean and atmosphere in the tropical regions year round and in the midlatitudes during the summer season. As a consequence, the impact of strongly coupled data assimilation is expected to emerge especially in these cases. As suggested by several studies (see, e.g., [Peña et al. 2003](#)) that identify ocean-driving areas in the tropics and atmosphere-driving areas in the extratropics, the stronger air-sea coupling found in the tropics, compared to the extratropics, may also be due to the thermodynamic-only nature of the NEMO-CheapAML coupling, which neglects feedback from wind anomalies.

To configure a variational assimilation system that embeds cross-medium balances, we adopt two possible approaches:

- 1) The use of statistical balances, which is straightforward to apply once a dataset representing background errors is given. In particular, we assume that anomalies with respect to the long-term mean may be representative of the model errors, as usually done in many ocean variational assimilation schemes.
- 2) The use of linearized ocean-atmosphere balance relationships, which come from the linearization of a set of bulk formulas around the background state. This second approach is a novelty of this work, aimed at demonstrating the feasibility of including balances coming from the linearization of strongly nonlinear flux formulations. Although the number of physical processes considered in our coupled model is limited,

this method partly mimics a possible configuration where air-sea balances come implicitly from the coupling of the tangent linear models inside the assimilation time window, as a natural extension of the use of the coupled model in the 4DVAR outer loops, recently proposed by [Laloyaux et al. \(2016a\)](#) for the CERA system.

Thus, the methodology proposed here represents a proof of concept of the use of coupled tangent linear models.

As a proof of concept, the strongly coupled data assimilation system has been used in a $1/2^\circ$ horizontal configuration to assess first the potential impact of the ocean-observing network on near-surface air temperature and humidity and later the impact of meteorological observations on the upper ocean. We have focused more on the former because the OceanVar data assimilation system was originally developed for ocean applications. Weakly coupled data assimilation is already able, in general, to project the ocean observations into the boundary layer through the air-sea heat flux exchanges within the forecast model because the assimilation time-window length and analysis frequency is daily, longer than in most NWP systems. For this reason, we did not find a significant impact of the data assimilation coupling strategy on long-term biases. Furthermore, an additional impact of strongly coupled data assimilation may arise from the assimilation of interface observations, such as satellite SST. These additional experiments are being considered at the moment, although optimal assimilation of swath SST data is nontrivial.

Results indicate that strongly coupled data assimilation is able, in many cases, to improve the skill scores against independent validation datasets. It is found that the impact grows with forecast range, suggesting that while at the beginning of the forecast time window, the impact is generally negative to neutral, probably requiring a further tuning of the cross-medium covariances implied by the strongly coupled DA system, after day 2 or 3 it reverts to positive. This has clear potential benefits for operational NWP forecast systems. In particular, we found in many areas (tropical Indian and Pacific Oceans and, to a lesser extent, midlatitudes and humidity skill scores) that the use of linearized air-sea balances derived from bulk formulas outperforms the use of simple statistical relationships. This result encourages further investigation of the possibility of using improved linearized air-sea balances: for instance, by relaxing the assumption of transfer coefficients independent of the oceanic and atmospheric states used here and implementing coupled linearized models (e.g., in the inner loops of four-dimensional variational data assimilation systems, such as CERA).

A number of weaknesses emerge, however, from this study, further to the simplistic use of the NEMO-CheapAML coupled model. We have in particular adopted background error covariances derived from monthly anomalies with respect to the long-term mean that were computed from simulations without any observational constraint. Although this is a common approach, it generally provides error covariances representative of large-scale and slow-varying processes, which may not be appropriate for our daily assimilation studies. Typically, error variances and spatial scales are overestimated in the tropical Pacific Ocean (e.g., [Storto et al. 2014](#)) with this method. In the future, techniques aimed at embedding smaller scales in the error covariances, such as the National Meteorological Center (NMC) method ([Parrish and Derber 1992](#)) or retrospective ensemble simulations ([Storto and Randriamampianina 2010](#)), may be used to shorten the time scales of errors. The use of monthly time scale covariances had, however, the advantage of neglecting any possible air-sea lag correlation, which should be accounted for when using short-range error covariances ([Lu et al. 2015](#)).

As a final remark, a mixed statistical-analytic operator may also be envisaged in the future, with a balanced component coming from the linearized air-sea relationships plus a purely statistical unbalanced component that uses hybrid vertical covariances. This possibility would mimic usual formulations adopted in both atmospheric (e.g., [Derber and Bouttier 1999](#)) and oceanic (e.g., [Weaver et al. 2005](#)) multivariate data assimilation systems and might further improve the initialization procedure.

Acknowledgments. This work has received funding from the EU FP7 ERA-CLIM2 project (Grant 607029). The EN4 subsurface ocean temperature and salinity data were collected, quality controlled, and distributed by the Met Office Hadley Centre. The altimeter products were produced by Ssalto/Duacs and distributed by AVISO, with support from CNES. The tropical mooring arrays data are provided by the TAO Project Office of NOAA/PMEL. Three anonymous reviewers and the editor are thanked for their valuable comments and corrections that contributed to improvement of the paper.

APPENDIX A

The Atmospheric Boundary Layer Model CheapAML

The CheapAML atmospheric boundary layer prognoses air temperature and specific humidity in the boundary layer (nominally at 2 m), considering advective, diffusive, and heat and moisture exchange

processes with the ocean and the free atmosphere. The model is coupled to NEMO, and it shares the same grid as NEMO, which in this study is a tripolar grid with an approximate resolution of 0.5° on the horizontal. All the details and assumptions of CheapAML are provided by [Deremble et al. \(2013\)](#). Here, we provide an overview of the boundary layer model. The governing equations are

$$\frac{\partial q}{\partial t} = -\nabla \cdot (q\mathbf{u}) + \nabla \cdot (A_h^q \nabla q) + \frac{E - \lambda P - F}{\rho_a h} \quad \text{and} \quad (\text{A1})$$

$$\frac{\partial T}{\partial t} = -\nabla \cdot (T\mathbf{u}) + \nabla \cdot (A_h^T \nabla T) + \frac{Q^{\text{sn}} + Q^{\text{ol}} + Q^{\text{il}}}{\rho_a c_a h}, \quad (\text{A2})$$

where A_h^q and A_h^T are the horizontal diffusivity for the specific humidity and temperature of air, respectively, both equal to $50\,000 \text{ m}^2 \text{s}^{-1}$. Parameter ρ_a is the air density (1.22 kg m^{-3}), h is the height of the atmospheric boundary layer, taken from ERA-Interim ([Dee et al. 2011](#)), and c_a is the specific heat of the air ($1000.5 \text{ J kg}^{-1} \text{ K}^{-1}$). Parameter E is the evaporation, P is the large-scale precipitation, F is the entrainment at the top of the boundary layer, \mathbf{u} is the boundary layer wind vector (from ERA-Interim), and Q^{sn} , Q^{ol} , and Q^{il} are sensible, outgoing longwave, and incoming longwave heat fluxes, respectively, where outgoing and incoming refer to the sea surface. The parameter λ regulates the amount of large-scale precipitation occurring at the top of the boundary layer, and it is set equal to 0.1.

The time stepping is actually split in the dynamical time step (9 s) and the thermodynamic one (1800 s). The advective trends are evaluated by a second-order centered scheme (leapfrog scheme).

Source and sink terms for the specific humidity are the evaporation E , equal to

$$E = \rho_a C_e (q_s - q) |\mathbf{u}| = \rho_a C_e [z \exp(-q_2/\text{SST}) - q] |\mathbf{u}|, \quad (\text{A3})$$

where C_e is the evaporation transfer coefficient, calculated according to [Large and Yeager \(2004\)](#), q_s is the saturation specific humidity, z is a constant equal to $514\,403.6 \text{ kg kg}^{-1}$, q_2 is equal to -5107.4 K , and $|\mathbf{u}|$ is the wind speed provided by ERA-Interim.

Parameter P is set equal to

$$P = \frac{\rho_a h}{\tau} (q - 0.7q_s) \frac{w}{w_0}, \quad (\text{A4})$$

where τ is the large-scale precipitation time scale (set to 6 h), q_s is the saturation specific humidity at the temperature T , w is the vertical wind, and w_0 is the vertical wind threshold ($0.75 \times 10^{-4} \text{ m s}^{-1}$). The entrainment at the top of the boundary layer F is equal to

$$F = \rho_a \mu C_e q |\mathbf{u}|, \quad (\text{A5})$$

where μ is the fraction of humidity entrained, set equal to 0.25.

For heat exchanges, the sensible heat flux Q^{sn} is computed as in [Large and Yeager \(2004\)](#), as

$$Q^{\text{sn}} = \rho_a C_h (\text{SST} - T) |\mathbf{u}|, \quad (\text{A6})$$

with C_h the sensible heat transfer coefficient ([Large and Yeager 2004](#)). Parameter Q^{ol} is the outgoing longwave radiation emitted by the ocean ($Q^{\text{ol}} = 0.96\sigma \text{SST}^4$), with σ the Stefan-Boltzmann constant ($5.67 \times 10^{-8} \text{ W m}^{-2} \text{ K}^{-4}$). Finally, Q^{il} is the incoming atmospheric longwave radiation, equal to

$$Q^{\text{il}} = -\frac{1}{2}\sigma T^4 - \frac{1}{2}\sigma T_h^4, \quad (\text{A7})$$

where the first right-hand side term accounts for atmospheric downward longwave radiation, and the second term accounts for the outgoing longwave radiation, with $T_h = T - (\gamma h)$ being the temperature at the top of the boundary layer and γ the atmospheric adiabatic lapse rate (0.0098 K m^{-1}). Note that the latent heat is assumed to propagate from the ocean surface above the atmospheric boundary layer; namely, it does not contribute to the heat exchanges.

APPENDIX B

Linearized Air–Sea Balance Operator

Air–sea exchanges are formulated by linearizing the bulk formulas of [Large and Yeager \(2004\)](#), with additional simplifications outlined below. Tangent linear freshwater fluxes δF are equal to the tangent linear evaporation flux δE , with the precipitation not depending on the ocean state:

$$\delta F = \delta E = \rho_a C_e [z q_2 \delta \text{SST} \exp(-q_2/\text{SST}_b) \text{SST}_b^{-2}] |\mathbf{u}|. \quad (\text{B1})$$

Parameter δSST is the tangent linear sea surface temperature, and SST_b is the background sea surface temperature from the nonlinear model trajectory.

Noting that the latent heat flux is assumed not to contribute to heat exchanges between the ocean and the atmospheric boundary layer and that the atmospheric longwave radiation does not depend on the ocean state, the air–sea heat fluxes δQ in the tangent linear model are given by the sum of ocean outgoing longwave radiative δQ^{ol} and sensible δQ^{sn} heat fluxes:

$$\delta Q = \delta Q^{\text{ol}} + \delta Q^{\text{sn}} = 4\sigma \text{SST}_b^3 \delta \text{SST} + \rho_a c_a C_h \delta \text{SST} |\mathbf{u}|. \quad (\text{B2})$$

A further simplification in the tangent linear air-sea flux operator of Eqs. (B1) and (B2) consists of assuming the transfer coefficients C_e and C_h are not dependent on the ocean state; that is, they are taken from the nonlinear model trajectory, implying that $\partial C_h / \partial \delta \text{SST} \simeq 0$ and $\partial C_e / \partial \delta \text{SST} \simeq 0$. This prevents the tangent linear version from using the highly nonlinear iterative procedure to calculate the nonneutral transfer coefficients of Large and Yeager (2004). In the future, weak dependence of the transfer coefficients on the sea surface temperature may be included, using simplified empirical relationships for the coefficients as in Kara et al. (2000), and in such case, Eqs. (B1) and (B2) should be modified accordingly. Tangent linear air temperature δT and specific humidity δq from the air-sea exchanges are, respectively, given by

$$\delta T = \Delta t \frac{\delta Q}{\rho_a c_a h} \quad \text{and} \quad (\text{B3})$$

$$\delta q = \Delta t \frac{\delta F}{\rho_a h}, \quad (\text{B4})$$

with Δt as the time step for the air-sea exchanges, set equal to 12 h, such that the increment δT matches the increment of the nonlinear model from a perturbation of sea surface temperature.

Adjoint balance routines were built starting from the tangent linear routines, following the rules of Giering and Kaminski (1998). Adjoint validation tests (see, e.g., Vidard et al. 2015) were implemented in OceanVar, and all the adjoint routines passed the tests successfully.

REFERENCES

- Barnier, B., and Coauthors, 2006: Impact of partial steps and momentum advection schemes in a global ocean circulation model at eddy-permitting resolution. *Ocean Dyn.*, **56**, 543–567, <https://doi.org/10.1007/s10236-006-0082-1>.
- Bernie, D. J., E. Guilyardi, G. Madec, J. M. Slingo, and S. J. Woolnough, 2007: Impact of resolving the diurnal cycle in an ocean-atmosphere GCM. Part 1: A diurnally forced OGCM. *Climate Dyn.*, **29**, 575–590, <https://doi.org/10.1007/s00382-007-0249-6>.
- Bishop, C. H., S. Frolov, D. R. Allen, D. D. Kuhl, and K. Hoppel, 2017: The Local Ensemble Tangent Linear Model: An enabler for coupled model 4D-Var. *Quart. J. Roy. Meteor. Soc.*, **143**, 1009–1020, <https://doi.org/10.1002/qj.2986>.
- Bouillon, S., M. Á. Morales Maqueda, V. Legat, and T. Fichefet, 2009: An elastic-viscous-plastic sea ice model formulated on Arakawa B and C grids. *Ocean Modell.*, **27**, 174–184, <https://doi.org/10.1016/j.ocemod.2009.01.004>.
- Buizza, R., and Coauthors, 2018: The EU-FP7 ERA-CLIM2 project contribution to advancing science and production of earth system climate reanalyses. *Bull. Amer. Meteor. Soc.*, <https://doi.org/10.1175/BAMS-D-17-0199.1>, in press.
- Byrd, R. H., P. Lu, J. Nocedal, and C. Zhu, 1995: A limited memory algorithm for bound constrained optimization. *SIAM J. Sci. Comput.*, **16**, 1190–1208, <https://doi.org/10.1137/0916069>.
- Courtier, P., 1997: Variational methods. *J. Meteor. Soc. Japan*, **75**, 211–218, https://doi.org/10.2151/jmsj1965.75.1B_211.
- Dee, D., and Coauthors, 2011: The ERA-Interim reanalysis: Configuration and performance of the data assimilation system. *Quart. J. Roy. Meteor. Soc.*, **137**, 553–597, <https://doi.org/10.1002/qj.828>.
- , M. Balmaseda, G. Balsamo, R. Engelen, A. J. Simmons, and J.-N. Thépaut, 2014: Toward a consistent reanalysis of the climate system. *Bull. Amer. Meteor. Soc.*, **95**, 1235–1248, <https://doi.org/10.1175/BAMS-D-13-00043.1>.
- Derber, J., and F. Bouttier, 1999: A reformulation of the background error covariance in the ECMWF global data assimilation system. *Tellus*, **51A**, 195–221, <https://doi.org/10.3402/tellusa.v51i2.12316>.
- Deremble, B., N. Wienders, and W. K. Dewar, 2013: CheapAML: A simple, atmospheric boundary layer model for use in ocean-only model calculations. *Mon. Wea. Rev.*, **141**, 809–821, <https://doi.org/10.1175/MWR-D-11-00254.1>.
- Dobricic, S., and N. Pinardi, 2008: An oceanographic three-dimensional variational data assimilation scheme. *Ocean Modell.*, **22**, 89–105, <https://doi.org/10.1016/j.ocemod.2008.01.004>.
- Donlon, C. J., M. Martin, J. Stark, J. Roberts-Jones, E. Fiedler, and W. Wimmer, 2012: The Operational Sea Surface Temperature and Sea Ice Analysis (OSTIA) system. *Remote Sens. Environ.*, **116**, 140–158, <https://doi.org/10.1016/j.rse.2010.10.017>.
- Farina, R., S. Dobricic, A. Storto, S. Masina, and S. Cuomo, 2015: A revised scheme to compute horizontal covariances in an oceanographic 3D-VAR assimilation system. *J. Comput. Phys.*, **284**, 631–647, <https://doi.org/10.1016/j.jcp.2015.01.003>.
- Fichefet, T., and M. A. Morales Maqueda, 1997: Sensitivity of a global sea ice model to the treatment of ice thermodynamics and dynamics. *J. Geophys. Res.*, **102**, 12 609–12 646, <https://doi.org/10.1029/97JC00480>.
- Fowler, A. M., and A. S. Lawless, 2016: An idealized study of coupled atmosphere-ocean 4D-Var in the presence of model error. *Mon. Wea. Rev.*, **144**, 4007–4030, <https://doi.org/10.1175/MWR-D-15-0420.1>.
- Frolov, S., and C. H. Bishop, 2016: Localized ensemble-based tangent linear models and their use in propagating hybrid error covariance models. *Mon. Wea. Rev.*, **144**, 1383–1405, <https://doi.org/10.1175/MWR-D-15-0130.1>.
- , —, T. Holt, J. Cummings, and D. Kuhl, 2016: Facilitating strongly coupled ocean-atmosphere data assimilation with an interface solver. *Mon. Wea. Rev.*, **144**, 3–20, <https://doi.org/10.1175/MWR-D-15-0041.1>.
- Giering, R., and T. Kaminski, 1998: Recipes for adjoint code construction. *ACM Trans. Math. Software*, **24**, 437–474, <https://doi.org/10.1145/293686.293695>.
- Good, S. A., M. J. Martin, and N. A. Rayner, 2013: EN4: Quality controlled ocean temperature and salinity profiles and monthly objective analyses with uncertainty estimates. *J. Geophys. Res. Oceans*, **118**, 6704–6716, <https://doi.org/10.1002/2013JC009067>.
- Han, G., X. Wu, S. Zhang, Z. Liu, and W. Li, 2013: Error covariance estimation for coupled data assimilation using a Lorenz atmosphere and a simple pycnocline ocean model. *J. Climate*, **26**, 10 218–10 231, <https://doi.org/10.1175/JCLI-D-13-00236.1>.

- Holt, T. R., J. A. Cummings, C. H. Bishop, J. D. Doyle, X. Hong, S. Chen, and Y. Jin, 2011: Development and testing of a coupled ocean–atmosphere mesoscale ensemble prediction system. *Ocean Dyn.*, **61**, 1937–1954, <https://doi.org/10.1007/s10236-011-0449-9>.
- Janisková, M., and P. Lopez, 2013: Linearized physics for data assimilation at ECMWF. *Data Assimilation for Atmospheric, Oceanic and Hydrologic Applications (Vol. II)*, S. Park and L. Xu, Eds., Springer, 251–286.
- Kanamitsu, M., W. Ebisuzaki, J. Woollen, S.-K. Yang, J. J. Hnilo, M. Fiorino, and G. L. Potter, 2002: NCEP–DOE AMIP-II Reanalysis (R-2). *Bull. Amer. Meteor. Soc.*, **83**, 1631–1644, <https://doi.org/10.1175/BAMS-83-11-1631>.
- Kara, A. B., P. A. Rochford, and H. E. Hurlbert, 2000: Efficient and accurate bulk parameterizations of air-sea fluxes for use in general circulation models. *J. Atmos. Oceanic Technol.*, **17**, 1421–1438, [https://doi.org/10.1175/1520-0426\(2000\)017<1421:EAABPO>2.0.CO;2](https://doi.org/10.1175/1520-0426(2000)017<1421:EAABPO>2.0.CO;2).
- Laloyaux, P., M. Balmaseda, D. Dee, K. Mogensen, and P. Janssen, 2016a: A coupled data assimilation system for climate reanalysis. *Quart. J. Roy. Meteor. Soc.*, **142**, 65–78, <https://doi.org/10.1002/qj.2629>.
- , J.-N. Thépaut, and D. Dee, 2016b: Impact of scatterometer surface wind data in the ECMWF coupled assimilation system. *Mon. Wea. Rev.*, **144**, 1203–1217, <https://doi.org/10.1175/MWR-D-15-0084.1>.
- Large, W. G., and S. G. Yeager, 2004: Diurnal to decadal global forcing for ocean and sea-ice models: The data sets and flux climatologies. NCAR Tech. Note NCAR/TN-460+STR, 112 pp., <https://doi.org/10.5065/D6KK98Q6>.
- Lea, D., I. Mirouze, M. J. Martin, R. King, A. Hines, D. Walters, and M. Thurlow, 2015: Assessing a new coupled data assimilation system based on the Met Office coupled atmosphere–land–ocean–sea ice model. *Mon. Wea. Rev.*, **143**, 4678–4694, <https://doi.org/10.1175/MWR-D-15-0174.1>.
- Le Traon, P.-Y., and F. Ogor, 1998: ERS-1/2 orbit improvement using TOPEX/POSEIDON: The 2 cm challenge. *J. Geophys. Res.*, **103**, 8045–8057, <https://doi.org/10.1029/97JC01917>.
- Lopez, P., 2016: A lightning parameterization for the ECMWF Integrated Forecasting System. *Mon. Wea. Rev.*, **144**, 3057–3075, <https://doi.org/10.1175/MWR-D-16-0026.1>.
- Lorenc, A., 1986: Analysis methods for numerical weather prediction. *Quart. J. Roy. Meteor. Soc.*, **112**, 1177–1194, <https://doi.org/10.1002/qj.49711247414>.
- Lu, F., Z. Liu, S. Zhang, and Y. Liu, 2015: Strongly coupled data assimilation using leading averaged coupled covariance (LACC). Part I: Simple model study. *Mon. Wea. Rev.*, **143**, 3823–3837, <https://doi.org/10.1175/MWR-D-14-00322.1>.
- Madec, G., and M. Imbard, 1996: A global ocean mesh to overcome the North Pole singularity. *Climate Dyn.*, **12**, 381–388, <https://doi.org/10.1007/BF00211684>.
- , P. Delecluse, M. Imbard, and C. Lévy, 1998: OPA 8.1 ocean general circulation model reference manual. IPSL Note du Pôle de Modélisation 11, 91 pp.
- Mahfouf, J.-F., 1999: Influence of physical processes on the tangent-linear approximation. *Tellus*, **51A**, 147–166, <https://doi.org/10.3402/tellusa.v51i2.12312>.
- McPhaden, M., and Coauthors, 1998: The Tropical Ocean–Global Atmosphere observing system: A decade of progress. *J. Geophys. Res.*, **103**, 14 169–14 240, <https://doi.org/10.1029/97JC02906>.
- Mirouze, I., and A. Storto, 2016: Handling boundaries with the one-dimensional first-order recursive filter. *Quart. J. Roy. Meteor. Soc.*, **142**, 2478–2487, <https://doi.org/10.1002/qj.2840>.
- Mochizuki, T., S. Masuda, Y. Ishikawa, and T. Awaji, 2016: Multiyear climate prediction with initialization based on 4D-Var data assimilation. *Geophys. Res. Lett.*, **43**, 3903–3910, <https://doi.org/10.1002/2016GL067895>.
- Mulholland, D., P. Laloyaux, K. Haines, and M. Balmaseda, 2015: Origin and impact of initialization shocks in coupled atmosphere–ocean forecasts. *Mon. Wea. Rev.*, **143**, 4631–4644, <https://doi.org/10.1175/MWR-D-15-0076.1>.
- Ngdock, H., M. Carrier, C. Rowley, T. Campbell, C. Amerault, L. Xu, and T. Holt, 2016: Development of a coupled atmosphere–ocean 4DVAR system. *Int. Workshop on Coupled Data Assimilation*, Toulouse, France, Météo-France, 14 pp., http://www.meteo.fr/cic/meetings/2016/CDAW2016/presentations/2_3.pdf.
- Parrish, D., and J. Derber, 1992: The National Meteorological Center's spectral statistical-interpolation analysis system. *Mon. Wea. Rev.*, **120**, 1747–1763, [https://doi.org/10.1175/1520-0493\(1992\)120<1747:TNC>2.0.CO;2](https://doi.org/10.1175/1520-0493(1992)120<1747:TNC>2.0.CO;2).
- Peña, M., E. Kalnay, and M. Cai, 2003: Statistics of locally coupled ocean and atmosphere intraseasonal anomalies in reanalysis and AMIP data. *Nonlinear Processes Geophys.*, **10**, 245–251, <https://doi.org/10.5194/npg-10-245-2003>.
- Penny, S., and Coauthors, 2017: Coupled data assimilation for integrated Earth system analysis and prediction: Goals, challenges and recommendations. WMO Tech. Rep. WWRP 2017-3, 59 pp., https://www.wmo.int/pages/prog/arep/wwrp/new/documents/Final_WWRP_2017_3_27_July.pdf.
- Rayner, N. A., D. E. Parker, E. B. Horton, C. K. Folland, L. V. Alexander, D. P. Rowell, E. C. Kent, and A. Kaplan, 2003: Global analyses of sea surface temperature, sea ice, and night marine air temperature since the late nineteenth century. *J. Geophys. Res.*, **108**, 4407, <https://doi.org/10.1029/2002JD002670>.
- Reynolds, R. W., T. M. Smith, C. Liu, D. B. Chelton, K. S. Casey, and M. G. Schlax, 2007: Daily high-resolution-blended analyses for sea surface temperature. *J. Climate*, **20**, 5473–5496, <https://doi.org/10.1175/2007JCLI1824.1>.
- Saha, S., and Coauthors, 2010: The NCEP Climate Forecast System Reanalysis. *Bull. Amer. Meteor. Soc.*, **91**, 1015–1058, <https://doi.org/10.1175/2010BAMS3001.1>.
- Sluka, T. C., S. G. Penny, E. Kalnay, and T. Miyoshi, 2016: Assimilating atmospheric observations into the ocean using strongly coupled ensemble data assimilation. *Geophys. Res. Lett.*, **43**, 752–759, <https://doi.org/10.1002/2015GL067238>.
- Smith, P., A. Fowler, and A. Lawless, 2015: Exploring strategies for coupled 4D-Var data assimilation using an idealised atmosphere–ocean model. *Tellus*, **67A**, 27025, <https://doi.org/10.3402/tellusa.v67.27025>.
- Stiller, O., 2009: Efficient moist physics schemes for data assimilation. II: Deep convection. *Quart. J. Roy. Meteor. Soc.*, **135**, 721–738, <https://doi.org/10.1002/qj.362>.
- Storto, A., 2016: Variational quality control of hydrographic profile data with non-Gaussian errors for global ocean variational data assimilation systems. *Ocean Model.*, **104**, 226–241, <https://doi.org/10.1016/j.ocemod.2016.06.011>.
- , and S. Masina, 2016: C-GLORSv5: An improved multipurpose global ocean eddy-permitting physical reanalysis. *Earth Syst. Sci. Data*, **8**, 679–696, <https://doi.org/10.5194/essd-8-679-2016>.
- , and R. Randriamampianina, 2010: Ensemble variational assimilation for the representation of background error covariances in a high-latitude regional model. *J. Geophys. Res.*, **115**, D17204, <https://doi.org/10.1029/2009JD013111>.

- , S. Dobricic, S. Masina, and P. Di Pietro, 2011: Assimilating along-track altimetric observations through local hydrostatic adjustment in a global ocean variational assimilation system. *Mon. Wea. Rev.*, **139**, 738–754, <https://doi.org/10.1175/2010MWR3350.1>.
- , —, and S. Dobricic, 2014: Estimation and impact of nonuniform horizontal correlation length scales for global ocean physical analyses. *J. Atmos. Oceanic Technol.*, **31**, 2330–2349, <https://doi.org/10.1175/JTECH-D-14-00042.1>.
- , —, and A. Navarra, 2016: Evaluation of the CMCC eddy-permitting global ocean physical reanalysis system (C-GLORS, 1982–2012) and its assimilation components. *Quart. J. Roy. Meteor. Soc.*, **142**, 738–758, <https://doi.org/10.1002/qj.2673>.
- Sugiura, N., T. Awaji, S. Masuda, T. Mochizuki, T. Toyoda, T. Miyama, H. Igarashi, and Y. Ishikawa, 2008: Development of a four-dimensional variational coupled data assimilation system for enhanced analysis and prediction of seasonal to interannual climate variations. *J. Geophys. Res.*, **113**, C10017, <https://doi.org/10.1029/2008JC004741>.
- Takacs, L. L., M. J. Suárez, and R. Todling, 2016: Maintaining atmospheric mass and water balance in reanalyses. *Quart. J. Roy. Meteor. Soc.*, **142**, 1565–1573, <https://doi.org/10.1002/qj.2763>.
- Vidard, A., P.-A. Boutrier, and F. Vigilant, 2015: NEMOTAM: Tangent and adjoint models for the ocean modelling platform NEMO. *Geosci. Model Dev.*, **8**, 1245–1257, <https://doi.org/10.5194/gmd-8-1245-2015>.
- Weaver, A. T., C. Deltel, E. Machu, S. Ricci, and N. Daget, 2005: A multivariate balance operator for variational ocean data assimilation. *Quart. J. Roy. Meteor. Soc.*, **131**, 3605–3625, <https://doi.org/10.1256/qj.05.119>.
- Zhang, S., M. J. Harrison, A. Rosati, and A. Wittenberg, 2007: System design and evaluation of coupled ensemble data assimilation for global oceanic climate studies. *Mon. Wea. Rev.*, **135**, 3541–3564, <https://doi.org/10.1175/MWR3466.1>.